POLITECNICO DI MILANO

School of Industrial and Information Engineering

Master Degree in Materials Engineering and Nanotechnology

Chemistry, Material and Chemical Engineering Department "Giulio Natta"

CAPILLARY BREAKUP AND ELECTROSPINNING OF PA6 SOLUTIONS CONTAINING IRON(III) CHLORIDE: EXPERIMENTAL FINDINGS AND CORRELATIONS

Supervisor: Prof. Francesco Briatico Vangosa
Co-Supervisor: Prof. Chiara Bertarelli

Master Degree Thesis:
Susanna Formenti
N° 782198

Academic Year 2012/2013

Table of contents

Figures

Graphs

Tables

Abstract

In this work the outcomes of the electrospinning of Polyamide 6 solutions in formic acid containing $FeCl_3$ are correlated with the rheological behaviour of these fluids, determined through the phenomenon of self-controlled capillary breakup of a filament. The rheological analysis enlightens a significant effect of the $FeCl_3$ content on the rheological behaviour, where the viscous component becomes predominant after a certain salt content threshold. At the same concentration the micrographical observations of the electrospun fibres show the formation of severely inhomogeneous structures. The adimensional analysis is used as tool to correlate the observations performed on the electrospinning results and the rheological behaviour of the solutions. To this end, the Elastocapillary number, index of the relative importance of viscous and elastic contributions to the flow, and the Deborah number, defined as the ratio between the polymer relaxation time and the characteristic time of the instability that causes fibre irregularities, are used. In particular, if Ec<1, the fibre morphology becomes significantly irregular, which implies the importance of the elastic component for the purpose of producing uniform fibres. The effect of this latter component is to induce a stabilization of the jet with respect to capillary instability, as suggests by the fact that uniform fibre morphologies are obtained for De>1. Besides the effect on the rheological behaviour, the fibre cristallinity seems to be affected by the $FeCl_3$ content, as above a critical concentration fibres turn out to be completely amorphous. Interestingly, this concentration coincides exactly with the one at which the viscous components starts dominating the rheological behaviour.

Sommario

Lo scopo di questo lavoro è correlare le caratteristiche delle fibre prodotte tramite elettrofilatura, a partire da soluzioni di Poliammide 6 in acido formico contenenti $FeCl_3$, con il comportamento reologico elongazionale delle stesse, determinato mediante la rottura autocontrollata di un filamento.

L'analisi reologica mette in evidenza un effetto significativo della concentrazione di $FeCl_3$ sul comportamento reologico, la cui componente viscosa diventa predominante oltre una soglia di concentrazione del sale. Alla medesima concentrazione l'osservazione microscopica delle fibre evidenzia la formazione di strutture fortemente non omogenee. Per correlare i due fenomeni si è fatto riferimento alla analisi adimensionale, considerando un numero Elastocapillare (Ec) – indice dell'importanza relativa dei contributi al flusso dei fenomeni elastici e viscosi – e un numero di Deborah (De) – rapporto tra tempo di rilassamento della soluzione e tempo caratteristico dell'instabilità capillare, che è causa dell'irregolarità delle fibre. In particolare, per Ec<1 la morfologia della fibra diventa significativamente irregolare, il che suggerisce l'importanza della componente elastica nell'ottenimento di fibre uniformi. Nello specifico, l'azione di tale componente consiste in una stabilizzazione dell'instabilità capillare, come suggerito dal fatto che solo le soluzioni caratterizzate da De>>1 consentono di produrre fibre uniformi.

Oltre all'effetto sul comportamento reologico, si è osservato che il contenuto di $FeCl_3$ influenza la cristallinità della fibre; difatti, esiste una concentrazione oltre la quale la cristallizzazione risulta impedita durante il processo di elettrofilatura. Sorprendentemente, essa coincide con quella a partire dalla quale la componente viscosa inizia a prevalere.

Introduction & aim of the work

In the last years, the nanotechnology field have been subjected to an ever growing attention by scientific and industrial research, thanks to the opportunity of producing objects with interesting features to be exploited in a broad range of applications. In particular, for what concerns polymer nanofibers, their use has appeared to be of great interest for several applications, thanks to their peculiar features, such as the high surface-to-volume ratio. Promising developments are being suggested by many studies in composite applications, production of filters, sensors, scaffolds and so on. For example, in sensor technology the extended specific area of nanofibers can greatly improve the speed and the responsiveness of the devices.

Currently, the electrospinning technique is the only one that allows the fabrication of continuous polymer nanofibers with complex architectures. In this process, an electrically charged jet erupts from a polymer solution droplet by means of an electric field, and it is elongated until it is finally collected in forms of micro or nano fibres on a grounded collector. Although this technique is rather easy to implement, in many cases it leads to unsatisfactory results; a well-known example is the so-called "beads on a string" structure, which can impair the performance of the obtained fibres, as it was observed that the latter is significantly influenced by the degree of fibre uniformity.

This said, it is clear that one of the main issues in the electrospinning technology concerns the control of the resulting fibres morphology. In dealing with this, one can in principle act on a wide series of parameters, such as solution surface tension and electrical conductivity, relative humidity and flow rate. However, as in most case non-newtonian fluids are used, the literature actually suggests that the formation of non-uniform structures is mainly related to the lack of elasticity of the polymer solutions.

Due to the complex rheological response exhibited by the kind of fluids adopted in this technology, their performances are generally described in terms of heuristic concepts,

such as 'spinnability' and 'stringiness'. Nevertheless, owing to the importance of the viscoelastic effects on the stability of the process, it is essential to follow a more exact way to quantify the degree of elasticity.

In order to do this, it is first necessary to examine what the electrospinning and, more in general, spinning process consists in, focusing on the rheological aspects. Basically, this process involves the formation, elongation and possible break up of a liquid filament. All these phenomena occur in free-surface elongational flow, during which the polymer solution undergoes capillary thinning. The different types of complex morphologies that can arise depend on the relative balance of capillary forces and fluid viscoelasticity, where the first drives the fluid thinning and eventually leads to the droplet formation, while the second opposes to this thinning and tends to lead to filament formation.

In light of this, in the literature some works relate the concept of spinnability to the presence of entanglements between macromolecular chains, which is strictly connected to polymer molecular weight and concentration. As a general remark, fluids are supposed to show a significant viscoelastic response only for concentration above the so-called critical overlap concentration for chain entanglements and are used consequently to be characterized merely through shear rheology. Nevertheless, it has to be borne in mind that the electrospinning process involves extensional deformations, thereby a method more apt for characterizing the rheological behaviour of the solutions needs to be adopted. Up to a short while ago, the elongational viscoelastic properties of polymeric solutions were neither considered to be essential, nor investigated in the context f electrospinning applications. Nowadays, the considerable progress that has been made in reproducing and modelling elongational flows can promote a better understanding about the underlying physical phenomena and may also be employed for the prediction of the process outcomes.

Some reliable measurements, both qualitative and quantitative, of fluid viscoelasticity in elongational flows can be carried out using extensional rheometers, which can be based on several different principles. Among them, the Capillary Breakup Extensional Rheometer is currently the most accurate commercially available instrument to carry out reliable measures of solution viscoelastic properties. The elegance of this technique lies in the simplicity of the procedure, in which the fluid is subjected to elasto-capillary self-thinning caused by an imposed step stretch deformation, and the evolution in the filament diameter is monitored as the slender thread undergoes necking and finally breaks. The transient diameter profile allows the evaluation of an apparent extensional viscosity, which characterizes the resistance of the fluid to stretching deformations. Moreover, modelling

the profile makes it possible to extract the intrinsic properties of viscoelastic fluids, such as the longest characteristic relaxation time and the elastic modulus. As reported in the literature, it is also possible to exploit the information obtained with the extensional rheometry by coupling them with other more conventional material properties, such as surface tension and shear viscosity. This approach allows defining some adimensional quantities, which can be promptly used not only to estimate the elasticity of polymeric solutions, but also to define an operating spinnability range for the electrospinning process.

In the wake of these considerations, the aim of the present work is to exploit the phenomenon of viscoelasto-capillary thinning in order to identify and extract important rheological information that could make the prediction of electrospun fibres morphology possible. To this end, a study of a novel system is presented: the attention is focused on polymer solutions of PA6 (Nylon 6) and iron(III) chloride hexahydrate ($FeCl_3$) in formic acid. As a matter of fact, the interest towards this system was tickled by the hypothesis that the ionic salt may disturb or even prevent H-bonds formation between amide groups of Nylon 6 backbones, and thus perturb solution viscoelasticity.

A systematic study was carried out at varying concentration of the salt in order to identify its effect on the rheological behaviour and on the spinnability of the system. To this end, a Capillary Breakup Extensional Rheometer (CaBER) was used to investigate the elongational behaviour of the solutions and to estimate which are the effects of the fluid properties, such as the longest polymer characteristic relaxation time, on the lifetime of a fluid thread undergoing capillary break-up. All the solutions were electrospun and the obtained fibres were analyzed on the basis of SEM images, to get information about their size and morphology. Furthermore, Differential Scanning Calorimetry was performed in order to gain information about the cristallinity of the nanofibers.

The rheological results interpretation was performed with the helpful tool of the adimensional analysis, that allowed determining a transition from a viscoelastic to a completely viscous behaviour about at 5,6% (wt/wt) $FeCl_3$ content. Below this threshold, the fluids turned out to be elastically dominated and stabilized, with a nearly constant relaxation time. Accordingly, uniform morphologies were observed from the SEM analysis of these solutions. Otherwise above the $FeCl_3$ critical concentration, the non-stabilized viscous fluids were unable to form fibres at all.

Moreover, an interesting observation was drawn from the calorimetric analysis. Above 4,5% $FeCl_3$ content, the electrospun fibres lost any cristallinity and thus became completely amorphous; this concentration interestingly corresponded to the threshold

above which the solutions started having an intermediate rheological behaviour, neither purely viscoelastic nor solely viscous. As a consequence, it seemed that, above a certain critical value, some correlation exists, between the effect of the salt in preventing H-bonds, as observed from rheology, and disturbing crystalline structure formation under stretching due to steric hindrance.

The work outline is presented hereby:

- chapter one is a brief overview on the electrospinning process and electrospun nanofibres;
- in chapter two, a bibliographic study on the elongational rheology of complex fluids in free surface flow is reported;
- chapters three and four include all the experimental details about the employed materials and methods;
- Finally, in chapter 5 the experimental results are presented and discussed.

Electrospinning

In the last years, the nanotechnology field have been subjected to an ever growing attention by scientific and industrial research, thanks to the opportunity of making products with interesting features to be exploited in a broad range of applications.

Focusing in particular on polymer nanofibers, the reduction of the diameter from micrometre to nanometre range involves the attainment of several interesting properties, among which the increase of the surface area to volume ratio (up to 103 times that of a microfiber), changes in the wetting behaviour and enhanced strength, as an effect of the strong decrease of the structural defects concentration on the fibre surface. These outstanding properties make these one-dimensional nanostructures of fundamental importance for application fields such as composite and biomedical industry, production of filter media, sensors, scaffolds and so on (Reneker, et al., 2007).

A wide number of methods have been already exploited for nanofibres synthesis and fabrication using several materials. Some examples are template synthesis, drawing, phase separation, self-assembly and electrospinning.

Among these processes, electrospinning represents a cost-effective and straightforward method, which allows for producing exceptionally long and uniform nanofibers and controlling their morphology simply by process parameter tuning. Moreover, this very flexible technique can be used to process a large set of polymers, such that up to recent days over 100 polymers have been employed, from natural to synthetic ones, alone or blended with other polymers or loaded with additives or nanoparticles.

At present, the demand of novel materials and the growing interest in nanotechnology has made the electrospinning process an excellent candidate for further developments concerning mass production of polymer nanofibres and fibrous structures. The notable interest in this techniques is testified by the fact that, although it was known already since

the early 30s, the number of publications featuring "electrospinning" as one of the key words has exponentially increased in these last years. Although this technique has not yet reached the industrial production, the promising potentialities of the electrospun structures have attracted attentions and investments all over the world. Hereafter, some applications are briefly highlighted in more detailed way Figure 1.1.
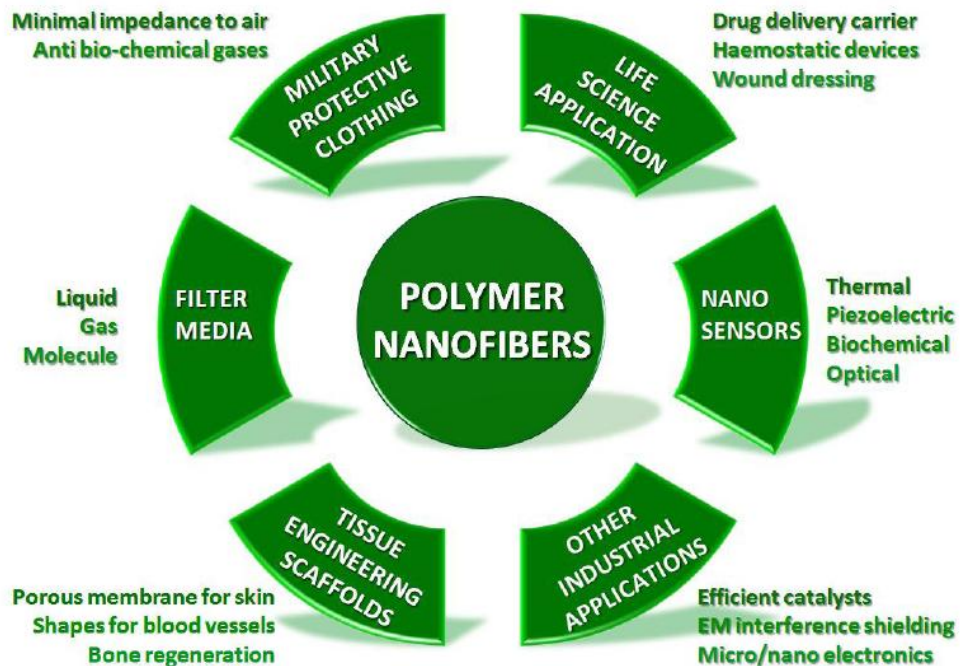
Figure 1.1 Potential applications of electrospun polymer nanofibers (Momentè, 2013)

One of the current major application of electrospun polymer nanofibers concerns **bioengineering**. Biocompatible nanofibers can be deposited as a thin porous film onto a hard tissue prosthetic device, working as an interface between the prosthetic device and the host tissues, in order to efficiently reduce the stiffness mismatch at the tissue/device interface. Moreover, they may be used to produce nanoscale fibrous scaffolds that can provide an optimal template for cells to seed, migrate, and grow. The employment of nanometer sized fibres has also been highlighted in developing high efficient **filter media**, due to the very high surface-to-volume ratio and resulting high surface cohesion, insomuch as tiny particles of the order of <0.5 μm can be easily trapped in the electrospun nanofibres structured filters. Conductive nanofibers might be employed for the production of tiny, light and flexible **electronic devices** or machines such as sensors and actuators. Furthermore, conductive nanofibrous membranes are also quite suitable as porous electrode in developing high performance battery and for potential application in electrostatic dissipation, corrosion protection, and electromagnetic interference shielding, photovoltaic device.

1.1. Process and parameters

The term "electrospinning" actually stands for "electrostatic spinning", and indeed it involves the production of nanofibres by means of an electrically charged jet of polymer solution at a pendant droplet (Formhals, 1934)(Formhals, 1944).

A standard experimental apparatus consists of a high voltage power supply, a syringe with a small diameter needle (spinneret) and a metal collector (Figure 1.2).
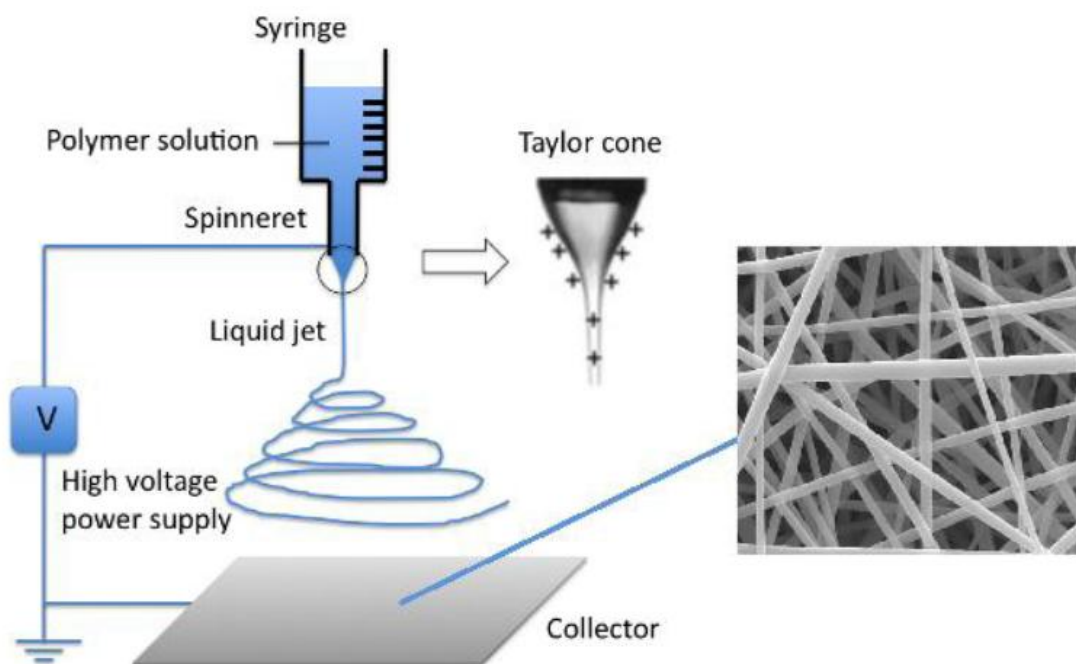
Figure 1.2 Electrospinning setup with magnification of the Taylor cone and of the fibre non woven mat collected (Li, et al., 2010)

During the process, a jet erupts from the tip of a polymer solution or melt pendant drop, which becomes unstable under the action of an electric field.

More specifically, an electric potential difference, around 10 kV, is set between an electrode in contact with the needle and another one connected to the collector, which is generally simply grounded. The polymeric fluid is extruded from the syringe at controlled flow rate and, when a droplet reaches the top of the needle, electrical charges are induced on the fluid surface by the action of the electric field. In the first stages, provided the potential is not too high, the droplet acquires a stable shape, resulting from the balance between the electric forces and the liquid surface tension, which tends to stabilize the hemispherical shape of the drop. When the charge repulsion reaches a critical value, at which any further increase will destroy the equilibrium, this electrostatic force opposes to the surface tension and, as the intensity of the electric field increases, it forces the

hemispherical surface of the drop at the needle tip to elongate, acquiring a conical shape, referred to as the Taylor cone. Finally, when the repulsive electrostatic force overcomes the surface tension, the fluid is drawn from the tip of this cone. In the first stages of its path, the solution jet flows nearly in a straight line, then it oscillates and deviates towards the collector into a complex path, undergoing the so-called whipping instability, during which the jet gets very long and thin due to the stretching imposed by electrical forces. During the jet flight towards the grounded collector, the solvent evaporates or melt cools down, so that polymer fibres are finally collected in the form of a solid interconnected web, usually referred to as "non woven fabric".

These electrospun polymer non-woven fabrics find several potential applications in the fields of bioengineering, energy and electronics, environmental engineering, defence and so on, as explained in detail in the previous section. Of course any application presents its specific requirements, to be fulfilled by appropriate properties. Nevertheless, in all cases the molecular structure, the mechanical properties and the morphology are of great interest (Ramakrishna, et al., 2005); among these, the latter, as shown by the literature survey, has a preeminent role in determining nanofibre performance. The average diameter and the possible amount of pores on the surface of a single fibre, as well as the porosity of membranes, need to be deeply investigated in order to assess fibre features. The employment of electrospun products requires them to be as uniform as possible, since the presence of a defect-rich structure will remarkably reduce fibre effectiveness.

Although this process seems rather easy to implement, there is a huge extent of different factors that play a role in affecting fibres formation and morphology and that must be taken into account to gain the desired results. Several works deal with the analysis of the effects of these factors, which can be broadly grouped into three main classes:

Polymer solution properties: polymer molecular weight, viscosity, polymer concentration, solution surface tension and electrical conductivity, solvent volatility.

Process conditions: voltage, flow-rate, gap (distance between the tip and the collector), needle diameter, hydrostatic pressure in the capillary tube.

Environmental conditions: temperature, relative humidity.

However, although all these factor are strictly interconnected, it is not possible to express rules of general validity that govern the process. Some operating parameters have to be experimentally defined and optimized for any different polymer-solvent system, in order to obtain uniform electrospun fibres.

The main effects of the mentioned parameters are explained below in details.

1.1.1.   Solution properties

As the polymer needs to be in a liquid form to be processed through the electrospinning technique, it follows that solution or melt properties play a primary role in determining fluid spinnability and fibre morphology.

Electrical property, surface tension and viscosity will determine the amount of stretching that could be imposed to the jet. Actually, they act together, but influencing the process in rather different ways. On one side, surface tension causes the liquid surface to neck, thereby reducing surface area and breaking the jet into droplets. On the other, the electrostatic repulsion between the charges leads to a local increase of surface area and the viscoelastic properties sustain and stabilize the jet, both preventing electrospraying and droplets formation. Moreover, also the rate of evaporation of the solvent results to be a key parameter, as it affects the viscosity of the solution during the flight towards the collector.

This said, the first way to control fibre morphology and reduce defects consists in selecting the right set of solution properties.

A high **surface tension** can be ascribed as the primary reason for the formation of beads along the jet, and so for a resulting non-uniform fibre morphology. The reduction of surface tension for gaining defect-free fibres can be achieved in different ways: using solvent with a low surface tension or adding surfactants to the solution is undoubtedly helpful. Moreover, the employment of a "good" solvent, so an enhanced polymer solubility, does have beneficial effects, also on solution viscosity.

Concerning solution **electrical conductivity,** as it increases more charges can be generated on the surface and carried by the jet. Of course, this means promoting jet formation and enhancing bending instability, and thence jet elongation. The system conductivity can be improved by employing solvent with higher dielectric constant. Also the addition of ionic salts may lead to the formation of uniform, defect-free and thinner fibres. When a small amount of salt is added to the solution, the increased charge density will allow for higher jet stretching, thus favouring smooth fibres formation and diameter reduction.

About this topic, an interesting study was carried out by Cai (Cai, et al., 2011): the effects of ferric chloride on electrospun polyacrylonitrile (PAN) composite nanofibers were investigated. Authors observed that morphology and average diameter of the electrospun PAN/FeCl$_3$ composite nanofibers were significantly affected by the ionic salt content. Basically, while the mean diameter of pure PAN nanofibers was in the order of some

hundreds of nm, by increasing the ferric chloride concentration up to 5% wt, the average diameter was decreased about four times.

Solution viscosity has already been told to be one of the most significant parameter in determining fibre morphology. When the role of this parameter is taken into account, it is worth noting that the usual measurements of shear viscosity are not enough to characterize the deformation behaviour of the polymeric fluid. In fact, in a technique such as electrospinning, the dominant mode of deformation is elongation rather than shear. This said, it is clear that a better interpretation of the process could be given considering the **extensional viscosity** of the solution. If the fluid is characterized by a purely viscous behaviour, namely it is Newtonian, the extensional viscosity is defined as three times the shear one; conversely, this is not correct anymore in presence of a non-Newtonian viscoelastic behaviour, in which the elongational response is essentially ruled by the degree of **elasticity** of the solution.

Moreover, the experience actually suggests that the occurrence of undesired non-uniform morphologies can be primarily ascribed to the lack of elasticity of the polymeric fluid (Yu, et al., 2006). As already discussed, the formation of droplets and beads is due to surface tension forces, that drives the so-called Rayleigh instability. If the viscoelastic polymer solution displays a sufficient degree of elasticity, the jet is stabilized by the built up of significant extensional stresses and the Rayleigh instability is either retarded or suppressed. Thence, whether the latter condition takes place, uniform fibre production does be realized.

Concerning this issue, it is a general belief that the degree of elasticity is mainly related to the polymer molecular weight and concentration, as far as they increase the extent of chain entanglements, which in turn efficiently improve solution viscoelastic response. As results, they actually have a significant impact on whether the morphology of the fibres results to be uniform or beaded. The density of chain entanglements is determined by the polymer molecular weight (MW), increasing for higher MW at fixed concentration. On the other hand, the entanglements density is enlarged also by the polymer concentration, for which a minimum value can be pointed out as threshold to stabilize the electrospinning process. From experimental studies on different polymer-solvent system (Shenoy, et al., 2005), it is shown that, below this critical value, the polymer is too dilute and there is not a sufficiently deformable network of polymeric chains and consequently droplets spraying is obtained. By gradually increasing the concentration, a beads-on-a-string structure is firstly formed, then beads tend to assume an elongated shape, until they finally disappear and continuous defect-free fibres are produced. Nevertheless, if the concentration is

further increased, the spinnability of the solution can be prevented due to too higher solution viscosity. The same morphological progression can be achieved by varying the polymer MW at fixed concentration.

However, in the literature (Yu, et al., 2006) it is reported that the presence of entanglements is a sufficient, but not necessary, condition for the fluid to develop strong elastic response. Strong elastic properties can actually be achieved for polymer concentration well below the critical overlap one, provided the longest fluid relaxation time, which is a measure of the solution viscoelasticity, maintains longer than the characteristic time of the process (i.e. extensional deformation). This kind of behaviour is typically shown by Boger fluids, that are excellent candidate for the purpose of investigating the effect of elasticity on electrospun fibre morphology, as they allow observing elastic properties independently of the other solution parameters (Yu, et al., 2006). This is basically achieved because of their peculiar property of making the recoiling phenomena slowing down thanks just too high solvent viscosity effect.

Since the solvent evaporates as the jet accelerates travelling towards the collector, also **solvent volatility** is indicated as a key solution parameter. When high boiling solvents are employed, they often lead to the deposition of wet fibres, which may stick together. On the other hand, low boiling temperature causes early solidification of the polymer solution, which may lead to further process instability or prevent an effective jet elongation and subsequent fibre shrinking. During the spinning process, phase separation may occur between the solidifying polymer and the evaporating solvent, which accumulates in some region, and affects fibre morphology Figure 1.3.
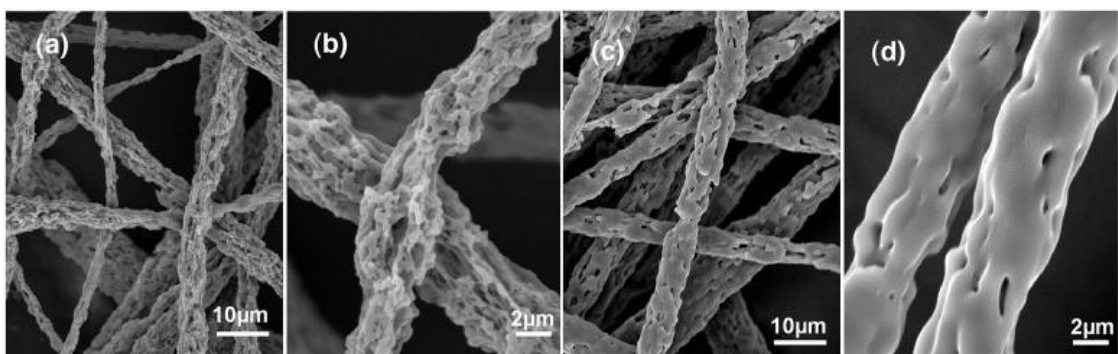
Figure 1.3 SEM images of porous fibres electrospun from a ternary system of butanol/ dichloromethane/poly-L-Lactide Acid at concentration of 8 WT% (Qi, et al., 2009)

1.1.2. Process conditions

Although the various external factors exerting on the electrospinning jet are less significant than the solution parameters, they have some non-negligible effects on the process itself.

Among them, the applied potential, responsible for inducing charges in the droplet solution and overcoming surface tension, have a non-univocal effect on the fibre morphology. Sometimes, a higher voltage seemed to promote the fibre elongation, making them more uniform (Figure 1.4), while in other cases rougher surface morphologies are obtained as the voltage increases.
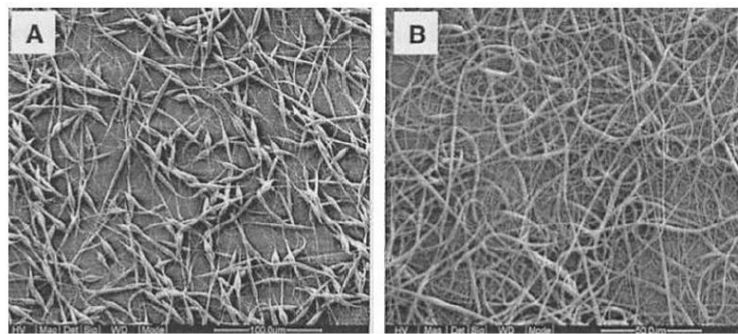
Figure 1.4 Polycaprolactone electrospun nanofibers at 6kV (A) and 22kV (B). (Qi, et al., 2009)

Moreover, increasing the voltage may lead to two opposite situations, that is either a diameter reduction or growth (Ramakrishna, et al., 2005). In fact, whether the voltage is increased, greater amount of polymer solution is drawn out of the spinneret, so a larger fibre diameter is expected to be observed, but contextually a stronger stretching action is imposed to the jet, resulting in the opposite effect. The dominant effect is actually defined accordingly to the polymer/solvent system and to the solution concentration. Anyhow, it has to be noticed that a better parameter that should be used might be the intensity of electric field, rather than the voltage.

For what concerns the flow rate of the polymer feed solution, an appropriate process range needs to be defined, since if it is too low, discontinuous production occurs, while for too high rate, the contact time between each fluid particle and the needle is not sufficient to let it charge, thus preventing the continuity of the jet.

The needle-collector distance affects the resulting morphology as far as it defines the travelling time of the jet. Higher gaps can be adopted in order to achieve both a complete evaporation of the solvent and a reduction of the mean diameter.

1.1.3. Environmental conditions

Nowadays, the effect of ambient parameters is still poorly investigated. Nevertheless, dealing with electrospun fibre morphology, the interaction between the jet and the surrounding environment is not negligible.

A high relative humidity causes formation of pores on fibre surface, as water tends to condense on it when the process is performed under normal atmosphere. This effect leads to the formation of the so-called "breath figures", where Vapour Induced Phase Separation (VIPS) occurs on the surface of the polymeric jet, leading to polymer-rich regions and polymer-poor regions in the thread Figure 1.5.
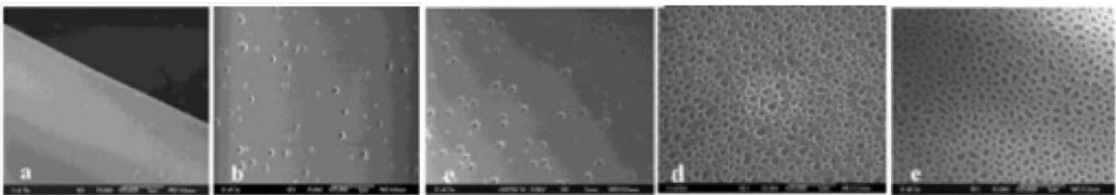
Figure 1.5 Morphology of polystyrene (PS) fibres obtained in different conditions of RH: (a) 25%; (b) 31-38%; (c) 40-45%; (d) 50-59%; (e) 60-72% (Casper, 2004)

Also a temperature effect may be anticipated, as temperature may change the evaporation rate of the solvent and also fluid viscosity, thus modifying the electrospun fibre formation.

1.2. Electrospinning of conductive polymers

As discussed above, electrospinning is a straightforward and easy to scale-up method to produce fibres with dimensions in the range of some μm down to few nm, featuring a high surface area and the possibility to be further functionalized. The high versatility of this technique makes it suitable for a wide range of applications and for the employment of numerous materials. In fact, since electrospinning basically consists in the drawing of a fluid, there are many different types of materials that can be electrospun, depending on the desired final application. Among them, three main classes can be identified, namely composites, ceramics and polymers.

Between the aforementioned materials, polymers are the more vastly used, including both synthetic and natural ones, copolymers and blends. Moreover, recently the scientific research is focusing an ever growing attention on the preparation of conducting polymer nanofibers via electrospinning(Liu, 2004)(MacDiarmid A., 2001)(Nair S., 2005), as this new class of organic materials shows the remarkable ability to conduct electrical current. However, processing of conducting polymers is not trivial, because of their relatively rigid backbones and limited solubility if compared to other synthetic polymers. In addition, getting electrospun fibres can be difficult, even though the parameters are in the required range for electrospinning. Further, even when fibre formation succeeds, the resulting fabric usually shows poor conductivity and mechanical strength. Finally, the conductivity was found to be very sensitive to the fibres morphology, which is related to the initial solution properties. Therefore, some strategies have been developed to overcome the issue, including the use of more flexible polymer precursors or even monomers, that can be converted into conductive polymer in a second step, and of a blend with a supporting spinnable non conductive polymer which assists the fibre formation(Di'az M., et al., 2001).

An example of conducting polymer that has lately triggered the research interest is polyaniline (PANI), as it is characterized by some peculiar features like ease of synthesis, excellent environmental stability and simple non-redox doping. Due to its noteworthy properties, PANI is being used in many applications, as related by several reports and review papers. Among them, sensors, membranes, conductive composite and surface and data storage are the main fields of interest.

Polyaniline is insoluble in most organic solvents and, as a result, an adopted strategy to produce nanofibres is the electrospinning of a common polymer, which acts as template, on which polyaniline is deposited by *in situ* polymerization in a second step (Hong, et al., 2005). However, it is reported that this approach showed a significant lack of reliability, as

uneven PANI coating resulted, mainly due to the absence of an opportune fibre functionalization, which leads to a poor growth control on the template. The system object of this study was devised to propose a novel contribution to this strategy. To this end, the presence of the ionic salt iron(III)chloride hexahydrate was exploited to get Nylon 6 electrospun fibres functionalized for further PANI polymerization.

Complex fluids

in free surface flows

In the previous chapter, the effect of the elastic component of the viscoelastic behaviour of a solution – often referred to as 'solution elasticity' in the literature – in the formation of electrospun fibres has been briefly highlighted. As mentioned, from the literature survey it is recognized that it plays a preeminent role in determining the feasibility of the electrospinning process and, in addition, in the production of fibre with uniform morphology, which is an essential feature for the purpose of enhancing fibre performance. This said, the need of investigating the extensional rheological behaviour of the solution undeniably arises, even though it actually appears to be all but trivial. Accordingly, the aim of this chapter is going into details of this topic, illustrating a novel method for the characterization of the extensional properties of polymer fluids.

2.1. Instability in liquid threads

The importance of the extensional behaviour of polymer fluids derives from the fact that several industrial processes, including blow moulding, extrusion, roll-coating and of course (electro)spinning, involve extensional deformations as the dominant mode (Sridhar, et al., 2002). The implementation of these processes is thus related to the dynamical response of an elongating filament and to the complex viscoelastic-flow instabilities that can be headed by the extensional rheological behaviour of the fluids.

As far as the electrospinning process is concerned, three types of flow instabilities may occur, namely Taylor, whipping and Rayleigh instabilities. Among them, the Rayleigh is the only undesired one, since its occurring leads to the necking and eventual breakup of the

liquid jet. As a consequence, it results to have a prevailing role in determining the feasibility of the process and the defects of the fibres. This instability was first described in 1878 by Sir Rayleigh, who examined the phenomenon of thin jets of fluids that become unstable and break into droplets (Figure 2.1). He demonstrated that the effect of gravity is negligible compared to surface tension for thread thin enough and how, if any perturbation happens to the filament, the jet changes its shape just in order to reduce the total surface energy, through minimizing its surface area. The perturbation can be basically described as a perturbation of the filament shape along its axis with a certain wavelength λ , thus the dynamics can be actually described in terms of characteristic length and time scales, deriving from energy and force balances. Carrying out some geometric and energetic considerations, it can be shown that a long cylindrical filament has a larger surface area than a sphere of the same volume, so that, when perturbed, it will tend towards assuming the energetically favoured spherical shape. Further, if the kinetics of the perturbation is taken into account, it follows that the jet will evolve into a row of droplets rather than a single big sphere, as this phenomenon takes a shorter time. The characteristic time for the instability to occur, which corresponds to the fastest growing wavelength, is set by the liquid rheology (Suo, 2004).
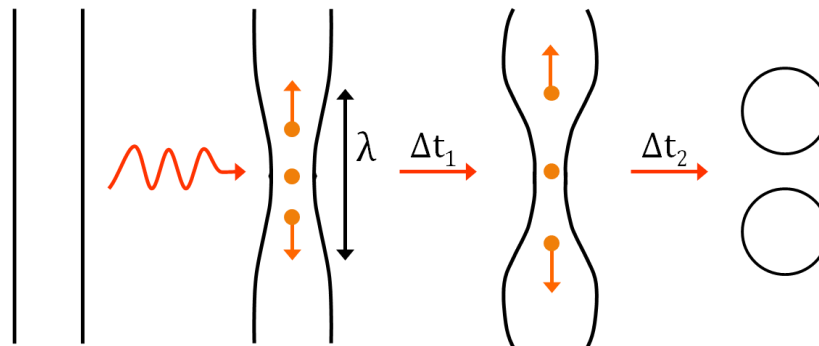
Figure 2.1 Rayleigh instability: evolution of a filament into droplets after a perturbation (wavy arrow)

Thus, no external forces act on the filament and nothing else but surface tension drives the necking instability, so as its dynamics is said to be a self-controlled or self-similar capillary thinning, since the fluid select its own time-scales. On the other hand, if kinetics is taken into account, the Rayleigh instability may be slowed down or even suppressed. In fact, it may happen that the fluid behaviour is such that viscous and/or elastic stresses can grow in the fluid filament during elongational flows. Whether these stresses are large enough, they can contrast the capillary action, leading to the stabilization of the jet. The evolution

of the filament profile thus depends on the relative importance of viscous and elastic contributions to the stress within the fluid thread and the capillary pressure.

Considering electrospinning, in this process the Rayleigh instability may take place in the solution jet during its travel towards the collector and this is the main cause for the occurrence of undesired non-uniform morphologies and even for the process unfeasibility. On the other hand, it can be stated that a pronounced viscoelastic behaviour of the fluid improves solution spinnability and electrospun fibre uniformity.

Indeed, studying unstable free surface extensional flows can be exploited as a method for extracting appropriate measures of the solution resistance to stretching and breakup (McKinley, 2005), and thus predicting, almost qualitatively, the results of the electrospinning process.

2.2. Self-controlled capillary breakup of a filament

Concerning free surface flows, there are many possible conformations of extensional flow that may be realized to reproduce self-controlled capillary breakup of a filament (i.e. the Rayleigh instability). Some examples are reported in Figure 2.2.
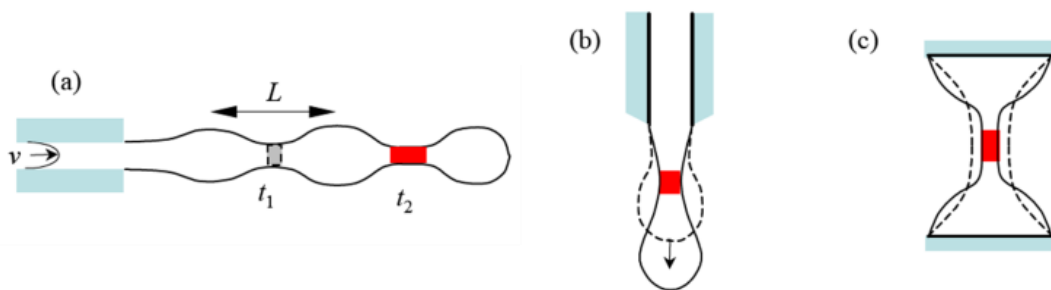
Figure 2.2 Three prototypical geometries for studying breakup of complex fluids; (a) continuous jetting instability; (b) dripping from a nozzle; (c) necking and breakup of a liquid bridge

Among the different geometries, the simple prototypical configuration, shown in Figure 2.2 (c), has been extensively studied in the last years. In this configuration, an unstable liquid bridge is initially formed after the rapid moving away of the two concentric and axisymmetric endplates that constrain the fluid. Once the plates stop, the imposed velocity is actually equal to zero and the thread evolution is purely controlled by the action of elastic, viscous, inertial and capillary forces(McKinley, 2005). The liquid bridge geometry exhibits the remarkable advantage that the material element at the neck is located at

approximately the same location of the laboratory reference system during the filament evolution, which makes the observation of its evolution in time quite easy.

This configuration has been exploited as the basis for the development of the Capillary Breakup Extensional Rheometry (CaBER), which is nowadays is one the few available techniques for measuring extensional behaviour of low viscosity liquid or solutions. The next sections illustrate the main CaBER features, in particular concerning the dynamics of the self-controlled capillary breakup phenomenon and the different approaches to be employed for modelling and extracting quantitative information about the fluid behaviour.

2.2.1. Modelling a thin filament capillary breakup: kinetics and force balance

In order to obtain useful material information from CaBER, it is essential to understand in detail the visco-elasto-capillary balance that governs the capillary thinning and breakup phenomenon. However, this is actually complex, since it requires a three-dimensional time-dependent approach. A widely used approximation consists in describing the self-controlled thinning phenomenon using a simplified one-dimensional approach. The thin filament can be described as consisting of cylindrical elements with radius $R(z)$ and height δ_z, each subjected to a purely extensional flow. It has to be noticed that this approximation is valid only in the slender central zone, and not near the plate regions.

The kinematics of the phenomenon can be described by a Lagrangian approach introducing the undeformed configuration, at which the fluid element is at Z_0 axial position (McKinley, 2005). After the stretch is imposed to the liquid column, each element that was originally at Z_0, is moved to a new z axial position (Figure 2.3), and subjected to a Lagrangian stretch S (Renardy, 1995) equal to:

$$S(Z_0,\mathrm{t}) \equiv \frac{\partial z}{\partial Z_0} = \frac{R_0{}^2}{R(z(Z_0),\mathrm{t})^2} \tag{2.1}$$

where $z(Z_0,\mathrm{t})$ is the Lagrangian position at time t of the one-dimensional element, originally located at time t_0 at the initial axial position Z_0, or equivalently to a Hencky strain of:

$$\varepsilon\left(Z_0,t\right) = 2\ln\left(\frac{R_0}{R(t)}\right) = \ln(S) \tag{2.2}$$

When the new configuration has been reached, each element goes on evolving with a strain rate $\dot{\varepsilon}$, defined as:

$$\dot{\varepsilon}\left(Z_0,t\right)=-\left.\frac{2}{R}\frac{\partial R}{\partial t}\right|_{Z_0} \tag{2.3}$$
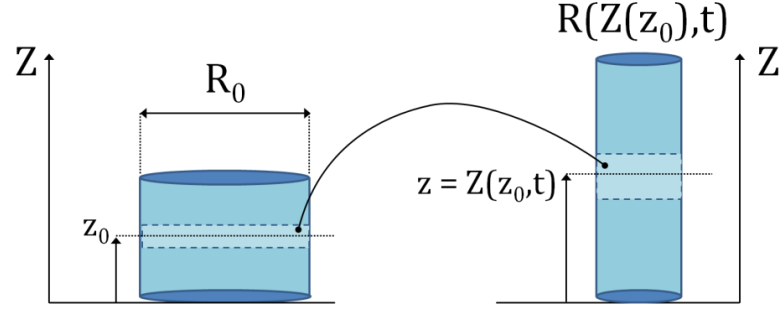
Figure 2.3 Undeformed configuration of a fluid column (left) and After the stretch: each element that was originally at z_0 is moved to a new z axial position

As regards the phenomenon dynamics, the expected form of the breakup profile can be obtained from a simplified one-dimensional form of the force balance on the thinning filament (McKinley, 2005)(McKinley, et al., 2000). Considering a fluid element of the filament, the stress balances in the axial (σ_{zz}) and radial (σ_{rr}) direction, if the stretch S is eliminated using equation 2.1 and the effects of higher order axial curvature (χ) and of axial gravity field are incorporated, are defined by the following expressions:

$$0=\frac{F_z}{\pi R^2}-2\eta_e\dot{\varepsilon}-\tau_{zz}+\frac{\rho g R_0^2 Z_0}{R^2}-p \tag{2.4}$$

$$-\frac{\sigma}{R}\chi=-\eta_e\dot{\varepsilon}-\tau_{rr}-p \tag{2.5}$$

where, in the experimental measurements, the radial profile $R=R(z(Z_0),t)$ is the primitive variable. In this description, the fluid quasi hemispherical droplets act as quasi-static reservoirs which absorb the fluid drained into them from the necking region and also alleviate the no-slip boundary condition at endplates. Instead, the boundary condition at the free surface sets the radial stress equal to the capillary pressure $p_{cap}=\sigma/R$.

In order to eliminate the hydrostatic pressure contribution, which otherwise cannot be evaluated, eq. 2.4 and 2.5 are subtracted and the following stress balance, containing all the forces acting on the fluid element, is obtained:

$$\eta_e \left\{ -\frac{2}{R}\left(\frac{\partial R}{\partial t}\right)_{Z_0} \right\} = \frac{F_z(t)}{\pi R^2} - \left[\tau_{p,zz} - \tau_{p,rr}\right] - \frac{\sigma}{R}\chi + \frac{\rho g R_0^2 Z_0}{R^2}$$

(2.6)

Moving left to right:

a. $\eta_e \left\{ -\frac{2}{R}\left(\frac{\partial R}{\partial t}\right)_{Z_0} \right\}$ represents the viscous extensional stress contribution to the extensional stress of a Newtonian fluid, with extensional viscosity $\eta_e = 3\eta_s$, or, considering a polymeric solution, of the viscous solvent;

b. $\frac{F_z(t)}{\pi R^2}$ is the force that is transferred from a fluid element to the next one and thus guarantees continuity in the liquid filament;

c. $\left[\tau_{p,zz} - \tau_{p,rr}\right]$ is the viscoelastic tensile stress contribution;

d. $\frac{\sigma}{R}\chi$ describes the effect of capillary pressure (i.e. surface tension) and the contribution arising from the mean radial and axial curvature of the filament (R' and R'' being $\frac{dR}{dZ}$ and $\frac{d^2R}{dZ^2}$) and $\chi = \left\{ \frac{1}{\left[1+\left(R'\right)^2\right]^{1/2}} + \frac{RR''}{\left[1+\left(R'\right)^2\right]^{3/2}} \right\}$;

e. $\frac{\rho g R_0^2 Z_0}{R^2}$ takes into account the body gravitational forces.

The a and c terms have to be evaluated using fluid constitutive models, that need to be specified based on the observed behaviour of the considered fluid. Once they have been obtained, combining them with the force balance equation allows writing a set of equations, which can then be solved analytically or numerically. The net force along the filament is not zero but is independent of spatial position, and thus it can be estimated by integrating the equation 2.6 along the length of the evolving fluid column.

For the purpose of further simplifying the analysis, it is useful to convert the equation 2.6 so that it contains only the midpoint thread radius R_{mid}. This can be done whether the

fluid thread is approximated as an axially-uniform cylindrical column of constant radius $R_{mid}(t)$, which is necking under the action of a capillary pressure, i.e. by assuming that the axial curvature is negligible. Furthermore, at late stages, the net tensile transferred force $F_z(t)$ approaches the value of the term due to surface tension:

$$\lim_{R_{mid} \to 0} F_Z(t) \to 2\pi\sigma R_{mid}(t)$$

(2,7)

Finally, provided that gravitational effect can be neglected[1], the following simplified equation, that describes the capillary breakup for all fluid type, is obtained:

$$-\frac{2\eta_e}{R_{mid}}\left\{\left(\frac{\partial R}{\partial t}\right)\right\} = -\left[\tau_{p,zz} - \tau_{p,rr}\right] + \frac{\sigma}{R_{mid}}$$

(2.8)

2.2.2. Capillary thinning of a viscous fluid

If the fluid undergoing the capillary breakup has a Newtonian behaviour, the equation 2.8 can be further simplified removing the viscoelastic term, obtaining the following equation (2.9) for the local force balance.

$$-\frac{6\eta}{R_{mid}}\left(\frac{\partial R}{\partial t}\right) = \frac{\sigma}{R_{mid}}$$

(2.9)

The integration of equation 2.9 with the initial condition $R_{mid}(0) = R_1$, where R_1 is the fluid thread radius just after the endplates stop, immediately leads to a linear decreasing profile:

$$R_{mid}(t) = R_1 - \frac{\sigma}{6\eta}t$$

(2.10)

---

[1] It is worth noting that the gravitational force term is zero under the condition that $Bo \gg 1$, where Bo is the Bond number, defined as $Bo = \dfrac{\rho g R_0^2}{\sigma}$.

Nevertheless, this formulation is not appropriate and consistent with experimental data (McKinley, et al., 2000). As a matter of fact, it can be applied only at the later stages of the phenomenon, when the gravitational effects are really negligible ($Bo \gg 1$). Moreover the axial force does not really reach the limiting value $F_z(t) = 2\pi\sigma R_{mid}(t)$. This issue can be overcome adjusting the assumption about the value of the net force along the filament, introducing a new dimensionless variable $X(t)$, defined as:

$$X(t) = \frac{F_z(t)}{2\pi\sigma R_{mid}(t)} \tag{2.11}$$

If $X(t)$ is constant, the following prediction for the time evolution in the midpoint radius is achieved:

$$R_{mid}(t) = R_1 - \frac{(2X-1)}{6}\frac{\sigma}{\eta}t \tag{2.12}$$

In the literature, several studies suggest different value for the X parameter; in case of an inertialess viscous fluid filament with smoothly necked profile, Papageorgiou defined $X = 0,7127$. On the other end, Eggers shows that in the very final stages, inertial effects can no longer be neglected and the change in the filament profile crosses over to a universal similarity solution that balances inertial, capillary and viscous effects, setting $X = 0,5912$ (Figure 2.4).
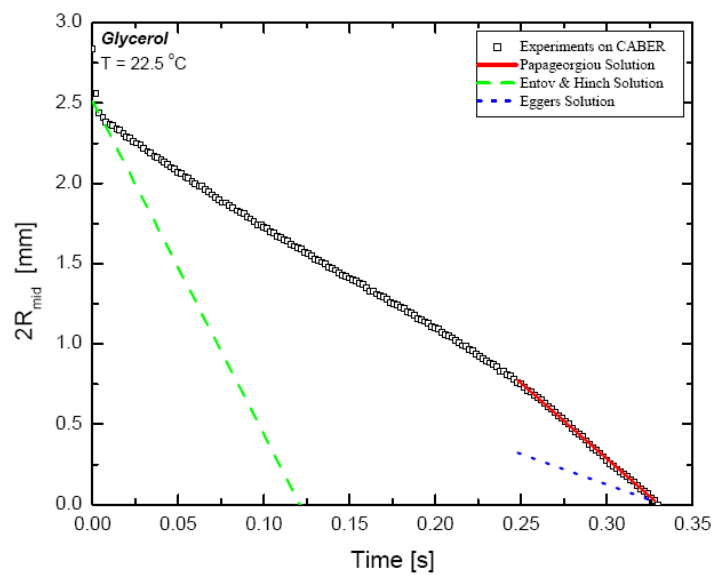
Figure 2.4 **Midpoint diameter evolution for glycerol together with the asymptotic prediction of the similarity solution of Papageorgiou and of eggers (McKinley, et al., 2000)**

2.2.3. Capillary thinning of a viscoelastic fluid

Dealing with a viscoelastic fluid, an appropriate constitutive equation has to be selected. As far as solutions are concerned, the literature reports two man choices, the Oldroyd-B and the FENE-P equations, characterized by one or more relaxation times. Among several examples, an interesting approach is proposed by Entov and Hinch (Entov, et al., 1997). They consider a discrete spectrum of relaxation times, with N modes having elastic moduli g_i and relaxation times λ_i, and assume that the modes arise from the response of N uncoupled FENE Dumbbells, with different maximum chain extension L_i.

Recalling that $\dot{\varepsilon}(t)$ is the axial strain rate of the axisymmetric extensional flow and under the unusual hypothesis of affine deformations, it is possible to define an axial deformation D_z^i and a radial deformation D_r^i, which describe each FENE kinematics according to:

$$\dot{D}_z^i = 2\dot{\varepsilon}D_z^i - \frac{f_i}{\tau_i}\left(D_z^i - 1\right) \tag{2.13}$$

$$\dot{D}_r^i = -\dot{\varepsilon}D_r^i - \frac{f_i}{\tau_i}\left(D_r^i - 1\right) \tag{2.14}$$

where the factor $f_i = \dfrac{L_i^{\,2}}{L_i^{\,2} + 3 - D_z^i - 2D_r^i}$ take into account the finite extensibility of the dumbbells mimicking the macromolecular chains. It must be borne in mind that $\dot{D}$ defined the kinematics of the macromolecular chains, while, macroscopically, the one of the liquid thread is still described by equation 2.3. Thus, each deforming dumbbell contributes to the stress balance with a force equal to $f_i g_i D_i$, provided that gravitational effect and axial curvature are neglected (assuming $p = 0$), the force balance obtained in the previous section becomes:

$$0 = \sigma_{zz} = -6\eta_s\dot{\varepsilon} + \sum_i f_i g_i D_z^i \tag{2.15}$$

$$-\frac{\sigma}{R} = \sigma_{rr} = -3\eta_s\dot{\varepsilon} + \sum_i f_i g_i D_r^i \tag{2.16}$$

As already mentioned, the axial stress σ_{zz} is supposed to vanish, due to the presence of the fluid drop reservoir at the stationary endplates, while the radial stress σ_{rr} are set equal to the surface tension by the boundary condition at the free surface. The equation 2.16 is studied through computational methods by Entov and Hinch (Entov, et al., 1997) considering a simple 8-modes model and then comparing the results of the simulations with experimental ones (Liang R.F., 1994), in order to verify the accuracy of the model. The integration is carried out setting as initial conditions:

$$R(0) = R_1 \tag{2.17}$$

with R_1 equals to the filament radius after endplate separation, and:

$$D_z^i(0) = 1 = D_r^i(0) \tag{2.18}$$

that means that, during the fast plate separation, dumbbells do not deform and all strain is accommodated by the solvent.

The result obtained with the multi-mode FENE approach is that the curve, describing the evolution in time of the thread radius $R(\mathrm{t})$, can be divided in three stages: the first, at very short time, of purely viscous adjustment, a middle one, dominated by the elastic behaviour, and, finally, the last one controlled by chain finite extension. Going into details, at early times, the elastic stresses are negligible, as they have no time to build up to a significant level. Thence, the initial stress is viscous and the phenomenon is ruled only by solvent viscosity and capillarity. Consequently, equation 2.16 reduces to:

$$\frac{\sigma}{R} = 3\eta_s \dot{\varepsilon} \tag{2.19}$$

and the decrease of the radius turns out to be linearly depending on time (eq. 2.20)(Figure 2.5), just as it was found in the previous section for the newtonian fluids.

$$R(t) = R_1 - \frac{\sigma}{6\eta_s} t \tag{2.20}$$

At the end of the first viscous stage, the elastic stress has grown to such an extent to be comparable with the capillary pressure and the viscous stress. The strain rate drops, so as

not to stretch the elastic stress beyond the capillary pressure, and the viscous stress drops too, as a result of the decrease in $\dot{\varepsilon}$; thus, the phenomenon can be described in term of a force balance just between elastic stress and surface tension. Furthermore, assuming that axial deformation of the modes is sufficiently large, $D_z^i >> 1 > D_r^i$, and that they remain small compared to the finite extension limit, $D_z^i << L_i^2$, so that $f_i \cong 1$, the new expression for the force balance becomes:

$$\frac{\sigma}{R} = \sum_i f_i g_i \tag{2.21}$$

Integrating equation with the initial conditions, the filament radius evolution in time is described by (Figure 2.5):

$$R(t) = R_1 \left(\frac{R_1 G(t)}{\sigma} \right)^{1/3} \tag{2.22}$$

where $G(t) = \sum_i g_i \exp\left(-\frac{t}{\lambda_i} \right)$ is a linear stress relaxation function for the fluid.
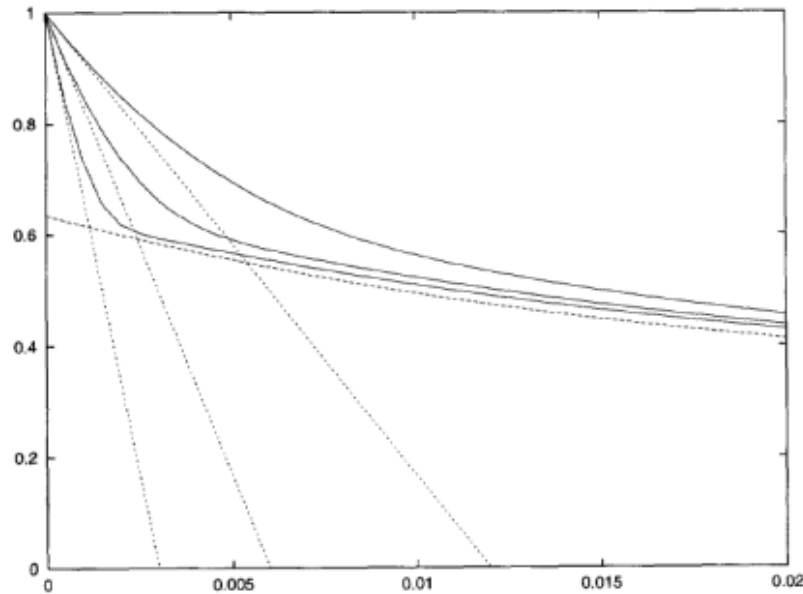
Figure 2.5 Evolution of the radius during time: the dotted lines are the asymptotic result of eq. 2.20 for early viscous time; the dashed line is the asymptotic result of eq. 2.22 for middle elastic time (Entov, et al., 1997)

From the numerical simulations, it also results that the stresses are dominated by the modes in succession and that dominant is the one with the relaxation time nearest to the considered time t. As a consequence, it can be shown that the strain rate, at which stresses

relax at time t, is $\dot{\varepsilon} = \dfrac{2}{3}\lambda$, namely two-thirds of the characteristic relaxation time λ of the dominant mode. Furthermore, Entov and Hinch state that it is possible to accurately represent the fluid behaviour using as spectrum only the dominant mode relaxation time λ, setting $g\lambda L = \sum_i g_i \lambda_i L_i$; accordingly equation 2.22 becomes:

$$R(t) = R_1 \left(\frac{R_1 g}{\sigma} \right)^{1/3} \exp\left(-\frac{1}{3}\frac{t}{\lambda} \right) \tag{2.23}$$

The validity of this one-mode model has been verified through the experimental study of some polystirenic based solutions (Anna, et al., 2001).

From a physical point of view, the exponential decrease of the radius involves that the filament thinning is quite gradual. Moreover, the presence of the elastic stresses not only stabilizes the capillary necking instability, but also forces the necked region to extend along the fluid thread (Figure 2.6). This phenomenon is qualitatively observed during experimental tests and justifies the already mentioned importance of viscoelasticity in process such as electrospinning. Additionally, these considerations explain the differences that can be observed in the qualitative evolving profile of the viscoelastic liquid bridge with respect to a purely viscous filament, in which the necking region lasts localized at the midpoint till the breakup event.
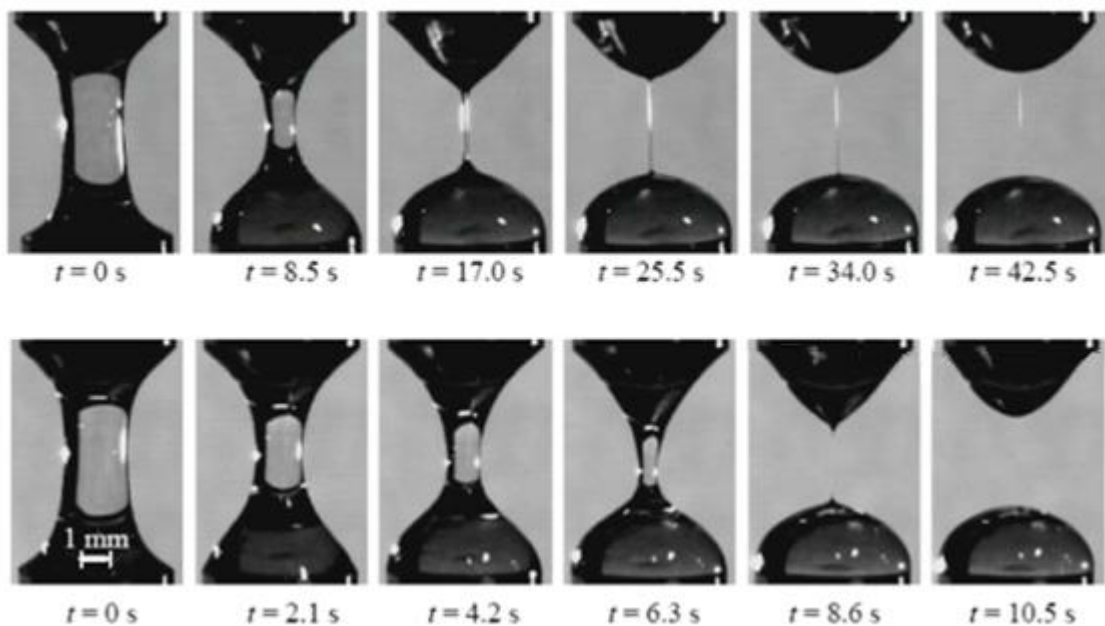
Figure 2.6 The evolving profiles of a viscoelastic liquid bridge (above) and a purely viscous filament (below)

35

At later stages, a change in the fluid behaviour is experimentally observed: as a matter of facts, the filament thinning phenomenon is faster than the prediction of equation 2.22, from which the critical time to breakup should be infinite. This condition may be verified only in some particular cases, as for solvents with low boiling point, that completely evaporate before the liquid thread have reached the breakup, thus leading to the formation of a solid filament. The FENE model allows to take into account this slowing down, thanks to the fact that Dumbbells - like the real macromolecules - reach the finite extension and the polymeric solution starts behaving like a suspension of rigid rods, oriented in the flow direction. Hence, the fluid is again approximated with a newtonian behaviour (eq. 2.24) (Figure 2.7).

$$R(t) = \frac{\sigma}{6\mu^*}(t - t_b) \qquad (2.24)$$

with $\mu^* = \frac{2}{3}\sum_i g_i \lambda_i L_i$.
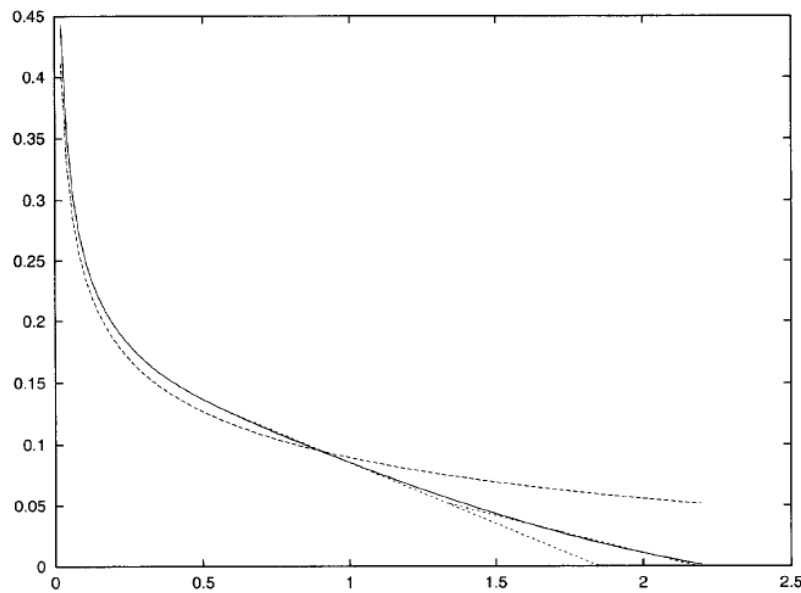
Figure 2.7 Evolution of the radius in function of time: the dashed line is the asymptotic result of eq. 2.22 for middle elastic time; the dotted lines are the asymptotic result of eq. 2.24 for finitely extensible dumbbells (Entov, et al., 1997)

2.2.4. Time-scales approach: adimensional analysis

The previous sections describe only two of the most-commonly observed modes of capillary thinning and breakup. Once the different behaviours have been accurately described and analyzed, in principle it should be possible to discriminate the most appropriate one from the observation of the self-controlled thinning, and assess whether a polymeric fluid is behaving as a purely viscous material or as a viscoelastic one. As a matter of fact, experimental reality is often far away from ideal cases: it is not so unusual, in particular for complex systems, to observe that a fluid chooses to behave 'midway'. Handling these situations is all but straightforward and frequently implies the urgency to look for a different method to single out fluid behaviours. To this purpose, a somewhat more qualitative approach can be implemented, exploiting the use of adimensional quantities. The tool of adimensional analysis is a good approach to deal with many other free-surface phenomena, that are used to be described by heuristic and poorly quantified concepts, such as 'spinnability', because of the difficulty in understanding them, coming from the large number of forces that may be involved.

The balance of forces controlling the dynamics of any process depends on the relative magnitudes of each underlying physical effect entering the set of governing equations. The basic concept of the adimensional analysis lies on the mutual comparison of the elementary phenomenon involved in the process, aiming at identifying the dominant one. Considering the specific case of self-thinning flows, it has to be noticed that, as mentioned, no external force is imposed, or better still, the dynamics that develop spontaneously in the fluid are much faster than any external applied force (McKinley, 2005). In such flows, the fluid thread thins and breaks up naturally under the action of capillary forces, setting its own evolution path on the base of its rheological behaviour, so it is necessary to seek a set of dimensionless parameters that depend on time scale rather than on velocity scale. In detail, capillary-thinning and breakup processes are governed by, at least, three characteristic time scales, that is a capillary (or Rayleigh), a viscous, and a polymer relaxation one. The first is defined as:

$$t_R = \sqrt{\frac{\rho l^3}{\sigma}} \qquad (2.25)$$

It is mainly related to surface tension σ and describes the characteristic time of the thinning and break up process, which is of Rayleigh instability. Note that l is the

characteristic length scale of the process. The viscous time scale t_{visc} includes the shear viscosity η_0 and depicts the effects of viscous forces in the fluid.

$$t_{visc} = \frac{\eta_0 l}{\sigma} \tag{2.26}$$

In the end, the polymer relaxation time, $t_{el} = \lambda$, defines the time scale for elastic stress growth in a uniaxial extensional flow (Rodd, et al., 2005) and gives indication about the degree of elasticity of the fluid.

The contributions of these effects to the total force balance can be inferred if the relative balances of the three time-scales are compared and can thus be represented in terms of three dimensionless parameters, defined as ratios between couples of characteristic times.

One of these is the *Ohnesorge Number*, Oh, that gives an estimate of the relative importance of the viscous stress with respect to capillary action, so as if it is greater than unity ($Oh > 1$), viscous effects dominate on the surface tension.

$$Oh = \frac{t_{visc}}{t_R} = \frac{\eta_0}{\sqrt{\rho \sigma l}} \tag{2.28}$$

Another important number is the ratio between the polymeric relaxation time to the Rayleigh one for capillary breakup. This parameter corresponds to an 'intrinsic' *Deborah number*, De, for free surface viscoelastic flows and describes whether elastic stress are large enough to dominate on capillarity (as for Oh, the condition is satisfied for $De > 1$).

$$De = \frac{t_{el}}{t_R} = \frac{\lambda}{\sqrt{\rho l^3 / \sigma}} \tag{2.29}$$

Finally, the elastocapillary number, Ec, represents the relative magnitude of elastic stress in the liquid thread with respect to the viscous one. If it is greater than one, then the elasticity is large enough to overcome the effect of the fluid viscosity. It is worth noting that Ec is actually nothing else but the ratio between Deborah and Ohnesorge numbers.

$$Ec = \frac{De}{Oh} = \frac{t_{el}}{t_{visc}} = \frac{\lambda \sigma}{\eta_0 l} \tag{2.30}$$

It has to be observed that until now the effect of gravity has been neglected in the adimensional analysis. However, this is justified considering that in most applications the characteristic lengths satisfy the condition for the gravitational forces to be neglected, being smaller than the *capillary length*, $l_{cap} = \sqrt{\sigma/\rho g}$, which is about 1-2 mm for most fluids.

The dimensionless number De and Oh can be exploited to define a two-dimensional operating space, which can be adopted to classify fluid behaviours and check their applicability in several process (Figure 2.8). In the case of CaBER, it requires the fluids to be 'sufficiently' viscous or elastic ($Oh > 1$ or $De > 1$), i.e. that either viscosity or elasticity resists the necking driven by surface tension. Furthermore, the bisector of this space results to be defined as $Ec = 1$, that means the presence of elastically dominated flows in the upper midplane ($Ec > 1$), and viscous dominated in the lower one ($Ec < 1$).
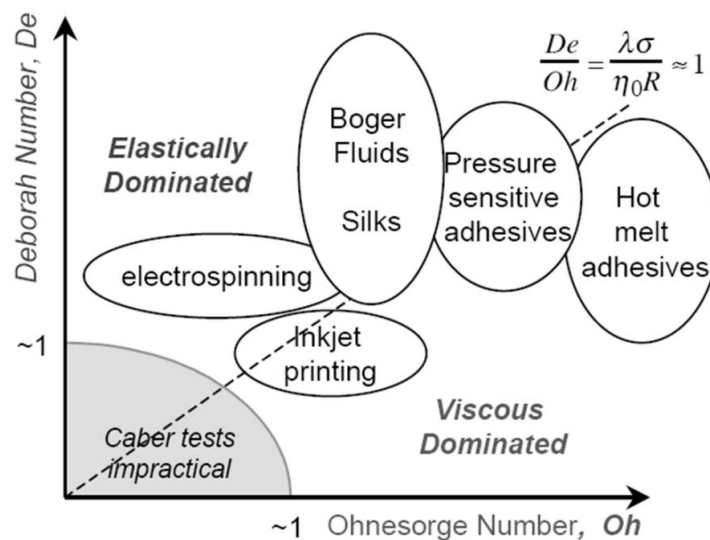
Figure 2.8 An 'operating diagram' for capillary self-thinning and break-up of complex fluids. regions for some common free surface flows are sketched

It has been already mentioned that in the electrospinning process the employed polymeric fluids need to be 'spinnable', thus characterized by a certain degree of elasticity, and be able to form uniform defect-free fibres. Consequently, the best operating condition can be achieved if the jet is both elastically dominated and stabilized, which means that De and Ec have to be greater than unity, as depicted in Figure 2.8. Moreover, as a general remark it is important to observe that in process such as electrospinning, where the characteristic length scale is decreased into the micro/nanometre range, inertial forces become

progressively less important and viscoelastic forces dominate, as all the three aforementioned adimensional numbers increase.

Investigated fluids

3.1. Solution composition

As already mentioned, this work aims at investigating the effect of the feed solution elasticity on the production of electrospun fibre webs.

In particular, it was decided to consider solutions of PA6 (Nylon 6) and iron(III) chloride hexahydrate ($FeCl_3 \cdot 6H_2O$) in formic acid. The choice of such a system was inspired by the work of professor Bertarelli's research group from the Department of Chemistry, Materials and Chemical Engineering of Politecnico di Milano, that was adopting the same solution to produce electrospun conducting nanofibers as templates for a successive in situ growth of polyaniline (PANI) (Momentè, 2013).

At length, iron(III) chloride hexahydrate is an oxidant salt, which contributes to increase the polymer solution conductivity and promotes PANI polymerization onto Nylon 6 fibre surface. On the other hand, $FeCl_3$ is a Lewis acid and thus can act on hydrogen bonding between amide groups of Nylon 6 backbones by disturbing or even preventing them (Starkweather Jr, et al., 1993) (Figure 3.1). In rheological terms, the consequences of the latter effect are all but trivial; however, this probably means that an increase in $FeCl_3 \cdot 6H_2O$ content reduces the fluid elasticity. Concerning this issue, the literature reports that the electrospun fibre morphology is significantly controlled by the fluid elasticity (Yu, et al., 2006), whose reduction negatively affects the electrospinning process, leading to the production of non-uniform fibres.
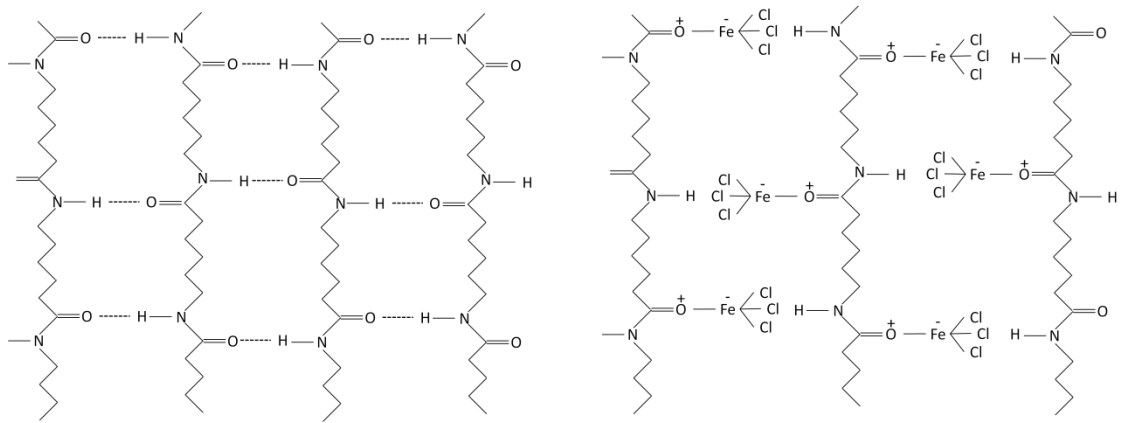
Figure 3.1 Effect of Fecl₃ on pa6 hydrogen bonds (dotted lines). left: hydrogen-bonded structure of PA6; right: non-hydrogen-bonded structure of PA6- FeCl₃ complex

This said, it is clear that the best condition will result from adjusting the content of iron(III) chloride, meaning having the largest amount of salt in solution without compromising the spinnability and the production of homogeneous and defect-free fibres.

Since it was the first time that this system was used in the electrospinning process, it was decided to carry out a methodical study on the content of $FeCl_3 \cdot 6H_2O$, in order to investigate the its effect on solution elasticity and on spinnability and fibre morphologies, and hence check if they are actually correlated.

3.2. Solution preparation

The procedure followed for the preparation of the test fluids consisted in two different steps: in the preliminary one, the polymer was dissolved in a specific solvent, then the salt was added and dissolved in the polymeric solution.

As already mentioned, formic acid was employed as solvent and Nylon 6 as polymer, at 15% (wt/wt) concentration with respect to formic acid. The PA6 pellets were weighted with an analytical balance (Mettler AE163) and then dissolved in 1mL of solvent by magnetic stirring at ambient temperature for about 1,5 hours.

Only after the polymer had dissolved, was iron(III) chloride hexahydrate ($FeCl_3 \cdot 6H_2O$) weighted and added to the polymeric solution, at concentrations ranging from 0% up to 10,3% (wt/wt with respect to formic acid). The solution underwent again magnetic stirring until complete dissolution of the salt, which required progressively longer times as the $FeCl_3 \cdot 6H_2O$ content was increased. The complete list of the tested solutions is

reported in Table 3.1. It has to be noticed that, since the FeCl$_3$ group is the one effectively interacting with the amide groups, from now on the solutions are referred to as the percentage by weight of the FeCl$_3$ content.

Table 3.1 Complete list of the solutions employed in the methodical study: for each solution, the weight percentage of hexahydrate and anhydrous FeCl$_3$ and the mass of the three components are listed

wt.% FeCl$_3$·6H$_2$O	0	1,6	2,4	3,2	4,0	4,7	5,5
wt.% FeCl$_3$	0	1	1,5	2	2,5	3	3,5
m Formic Acid	1 ml	1 ml	1 ml	1 ml	1 ml	1 ml	1 ml
m PA 6	0,183 g	0,183 g	0,183 g	0,183 g	0,183 g	0,183 g	0,183 g
m FeCl$_3$·6H$_2$O	--	0,019 g	0,029 g	0,039 g	0,048 g	0,056 g	0,068 g
wt.% FeCl$_3$·6H$_2$O	6,3	7,1	7,9	8,7	8,9	10,3	
wt.% FeCl$_3$	4	4,5	5	5,5	5,6	6,5	
m Formic Acid	1 ml	1 ml	1 ml	1 ml	1 ml	1 ml	
m PA 6	0,183 g	0,183 g	0,183 g	0,183 g	0,183 g	0,183 g	
m FeCl$_3$·6H$_2$O	0,077 g	0,086 g	0,096 g	0,106 g	0,108 g	0,125 g	

Dealing with the preparation of these systems actually required some efforts, as the feed solutions maintained their characteristics and spinning ability just over some hours, after which fluid alterations occurred. This could be observed as the solutions, originally dark-orange coloured, turned yellow (Figure 3.2), probably because of water absorption from the surrounding environment, promoted by the hygroscopic character of the iron(III) chloride. A proof of the accuracy of these qualitative observations was given by the rheological measurements performed on a solution at 5,6% FeCl$_3$, previously aged for two days. Before testing, the sample appeared to be yellow, and indeed the behaviour of the solution turned out to be significantly different from the corresponding non-aged one (Figure 3.3). Furthermore, the alterations actually led to a drop of viscosity and elasticity, which is absolutely not a desirable effect. Therefore, all these issues related to solution preservation had implied that the sample solutions had to be prepared right before they were used.
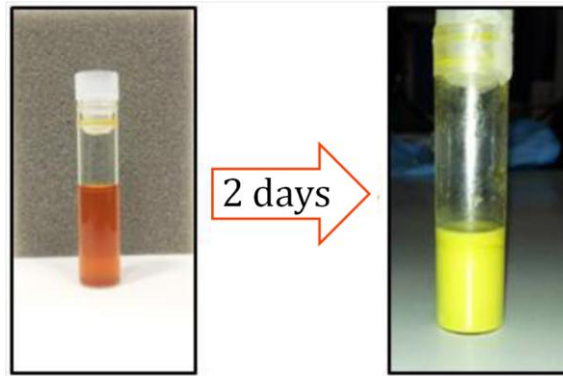
Figure 3.2 Photo of the 5,6% FeCl₃ solution aged for two days (right); the left image represents the same solution right after the preparation
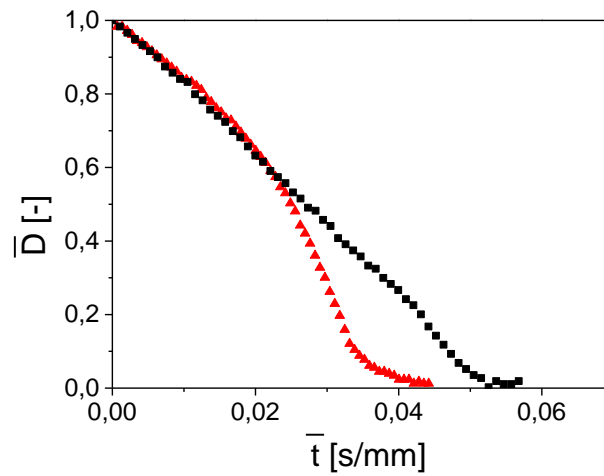
Figure 3.3 Diameter evolution curves of 5,6% FeCl₃ solutions: the red curve represents the 2days-aged one and it can be observed that it is characterized by a more viscous behaviour with respect to the black non-aged solution

Experimental methods

The aim of this chapter is to give an overview on the experimental methods that have been adopted throughout this work (Figure 4.1).

First of all, it has to be specified that, once the solution had been prepared, part of it underwent capillary breakup extensional rheometry characterization, to investigate the extensional rheological properties of the fluids, while the remaining part was employed for the electrospinning process, to produce nanofibres web. Concerning the electrospun fibres, they were later characterized by Scanning Electron Microscopy and Differential Scanning Calorimetry, in order to obtain respectively information about fibre dimension and morphology and about material cristallinity.

Furthermore, other more conventional solution characterizations were performed, so as to get all the measurements required for a correct interpretation of the experimental results.
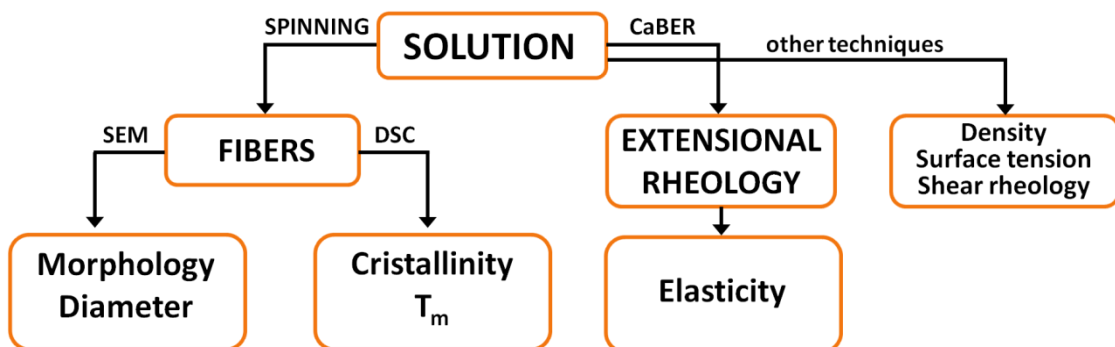

Figure 4.1 Outline of the experimental methods adopted throughout the work on PA6-iron(III) chloride systems

4.1. Capillary Breakup Extensional Rheometry

As mentioned above, the capillary breakup extensional rheometry measurements were exploited as means to investigate the extensional rheological properties of the solutions.

This is pursued by placing a nearly cylindrical fluid sample between two cylindrical endplates which are then rapidly separated by an imposed axial step-strain. The initial axial separation of the plates may be viewed as the elongational equivalent of a "step–strain" experiment, provided that the separation rate is much faster than the viscoelastic fluid relaxation time and the timescale for capillary drainage (Anna, et al., 2001). On stretching, an elongated hour-glass shaped liquid bridge forms between the plates; after the stretching stops, the capillary pressure causes a progressive thinning of this filament, in which a uniaxial extensional flow is produced. If the liquid thread eventually reaches the breakup, two separated drops are left on the plates (Figure 4.2).
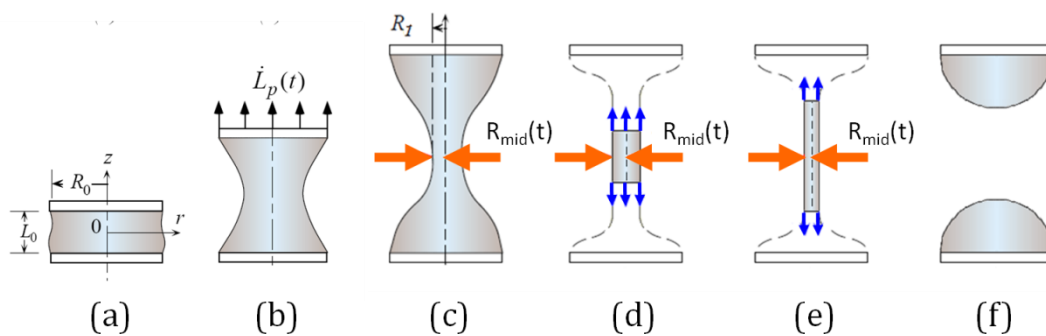
Figure 4.2 Schematic diagram of operation of a liquid filament rheometer and subsequent visco-elasto-capillary drainage of the fluid column: (a) initial configuration of liquid column; (b) imposed stretching deformation and liquid bridge formation; (c) measurement of visco-elasto-capillary drainage of the slender necked filament using a laser micrometer at the axial midplane ; (d-e) axially uniform fluid thread; (f) drop formation after the breakup event

It is also worth noting that in this technique the minimum radius is constrained to be close to the midplane of the thread by geometry and by initial step-strain, unless for very large imposed strain and important gravitational drainage (Rodd, et al., 2005). Therefore, by monitoring the evolution of the thread midpoint diameter, it is possible to make qualitative observation about the extensional behaviour of the fluids and even to extract quantitative about the extensional rheological properties of the fluids, if an appropriate constitutive equation is chosen to describe the fluid behaviour.

4.1.1.   Instrumentation and experimental setup

The commercial available HAAKE CaBER 1 (Thermo Fisher Scientific) was used as capillary breakup extensional rheometer (CaBER). It essentially consists of two cylindrical plates between which the fluid sample is loaded, a closed temperature-controlled sample chamber, a linear motor drive with variable speed that control the plate motions and a class 1 laser micrometer to measure the diameter evolution in time (Figure 4.3).
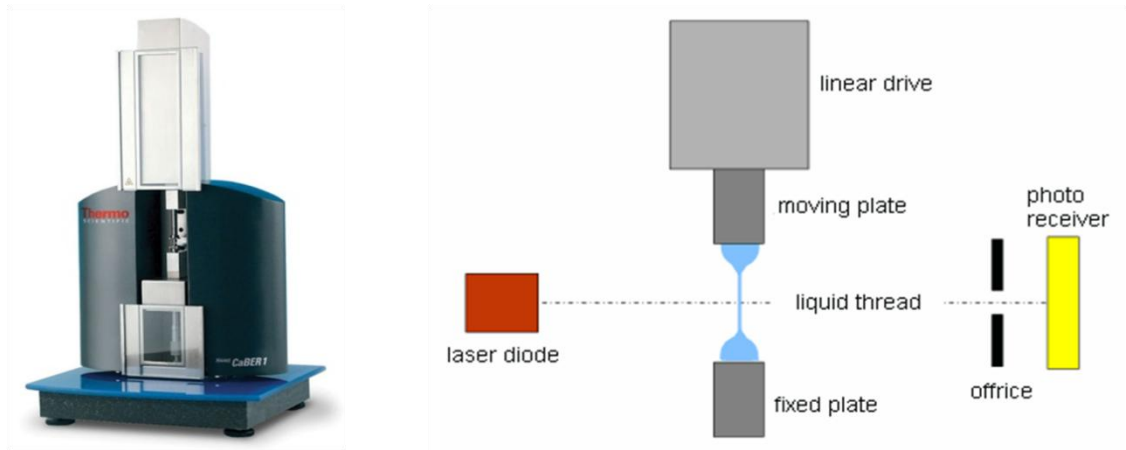

Figure 4.3 The CaBER apparatus

The history of the endplate separation determines the imposed strain history; more specifically, three types of histories are available to approximate the desired step-strain: linear, exponential or cushioned strike (Figure 4.4). In the present work, the cushioned profile, with a strike time of approximately 20 ms, was adopted for all the measures. The exponential deceleration at the end of the motion should help to reduce the problems caused by fast deceleration.
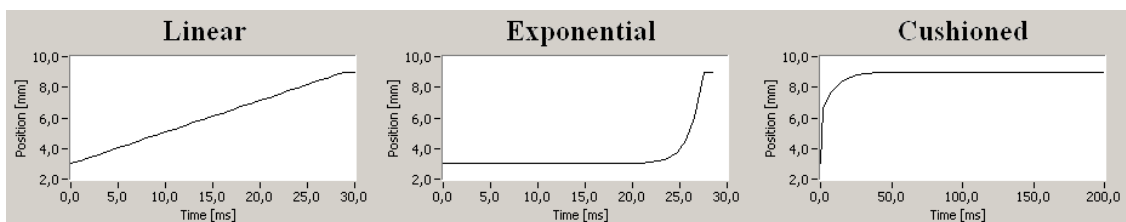

Figure 4.4 Schematic representation of the three types of histories available to approximate the initial step-strain: moving left to right, linear, exponential and cushioned strike

The plate diameter, for which three dimensions are available (4, 6 or 8 mm), together with the initial plate separation length, defines the volume of the fluid sample, while the combination of the initial and final upper plate position determines the extent of imposed

deformation. The nominal imposed Hencky strain is defined as $\hat{\varepsilon}_H = \ln\left(\frac{\Lambda_1}{\Lambda_0}\right)$, where the aspect ratio Λ_0 is defined as the ratio between the plate radius and the initial sample height, corresponding to the initial separation length, $\Lambda_0 = L_0/R_0$, while Λ_1 is the ratio between the plate radius and sample height after the step-stretch, $\Lambda_1 = L_1/R_0$.

Dealing with all these experimental parameters, some preliminary tests had to be carried out on two solutions (namely 0% and 5,6%), in order to optimize the testing conditions for the studied system. The adopted setup conditions, for all the solution characterizations, are listed in Table 4.1.

Table 4.1 Setup conditions adopted for the solution characterization

Plate diameter, D_0	Initial length, L_0	Final length, L_1	Hencky strain, $\hat{\varepsilon}_H$	Profile
6 mm	1 mm	6 mm	1,77	cushioned

The CaBER tests were performed in a thermostatic lab, with controlled temperature. The temperature of the sample chamber was controlled by cryostat and set at 25°C; nevertheless, the tests had actually been performed keeping the chamber open, as it is explained in the next section.

For each solution, the test was performed eight times, each one using a different sample, in order to obtain a suitable number of data to evaluate the accuracy and the repeatability of the measurements.

4.1.2.   Diameter evolution monitoring technique

Referring to the analysis of breakup phenomenon reported in chapter 2, it is evident that the filament diameter after the plate separation (D^*) is a key parameter for the purpose of experimental result interpretation. Thence, this quantity have to be evaluated in the most accurate and unambiguous possible way.

The HAAKE CaBER software does extract a value for D^*, combining the linear motor drive position data and the data acquired by the laser micrometer. Nevertheless, considering the importance of this parameter, it was decided to try to validate the software output by carrying out some tests and simultaneously recording them with a high speed camera. This procedure would actually allow making a comparison between the diameter value obtained from the software and the one evaluated from the image processing.

The D^* validation tests were carried out on two different sample fluids, already being used for another study: a standard newtonian fluid, S8000 (Cannon Instrument Company), and a polymeric solution of cellulose acetate in ethyl lactate (10% wt/wt), referred as C225. The testing conditions for both fluids are reported in Table 4.2.

Table 4.2 Testing conditions for the model fluids S8000 and C225

	Plate diameter, D_0	Initial length, L_0	Final length, L_1	Hencky strain, $\hat{\varepsilon}_H$	Temperature	Profile
S8000	6 - 4 - 8 mm	3 mm	12 mm	1,3	35°C	cushioned
C225	6 mm	2,5 mm	8 mm	1,2	10-20-30-40°C	cushioned

The tests were reported with custom built high speed camera system at 500 fps frame rate (frame size: 1000x1000 pixel), using Micro Nikkor 5 mm lens. A video processing software (VirtualDub) was employed to extract the desired frame, and then the filament diameter was evaluated from the frame image using the ImageJ software.

What actually resulted from the comparison of the D^* values, both from video processing and CaBER output, was that the former one was always smaller. This can be probably explained by the fact that, due to inertial effects, the upper plate did not end its motion when it was supposed to do, but it had a small downwards return, during which the filament thinning kept on occurring. A further proof of this observation derives from the fact that the D^* difference was found to be greater for the C225, which diameter evolution was indeed quite faster compared to the S8000 one. As a consequence, the value determined by the CaBER software turned out not to be reliable and an alternative way to determine D^* has to be exploited.

One possible strategy is suggested by the literature (Spiegelberg, et al., 1996). In Spiegelberg's article it is proposed that during the plate separation the filament diameter basically evolves with an exponential decay, described by the following equation:
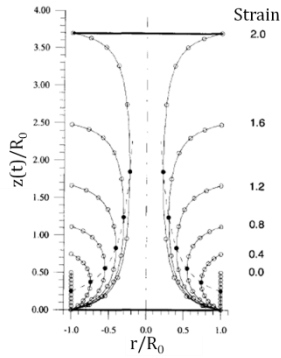
$$\frac{D_{mid}(t)}{D_0} = e^{-\frac{3}{4}\dot{\varepsilon}t} \qquad (4.1)$$

where $\dot{\varepsilon}$ is the constant plate separation rate and the quantity $\dot{\varepsilon}t$ corresponds to the instantaneous deformation of the liquid column during plate separation, defined as:

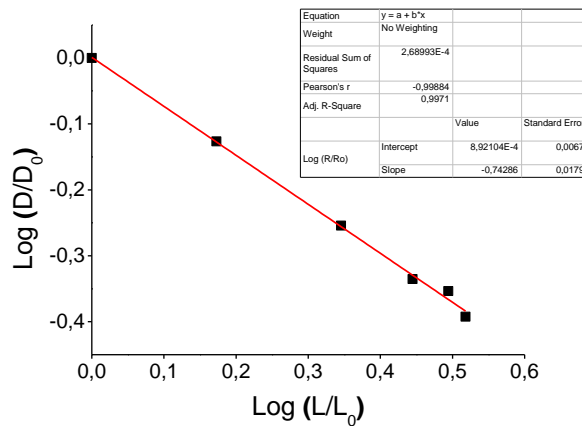$$\dot{\varepsilon}t = \frac{L(t)}{L_0} \qquad (4.2)$$

This means that D^* can be defined as D_{mid} at the end of the plate motion and it can be evaluated from the initial diameter, which actually results equal to the plate diameter, under the assumption that the solution is properly loaded between the plates.

The reliability of this approach was verified on the results obtained for the S8000 and C225 samples. For each test, six frames were extracted from the video during the plate separation stage, approximately at constant time intervals between successive frames (Figure 4.5).
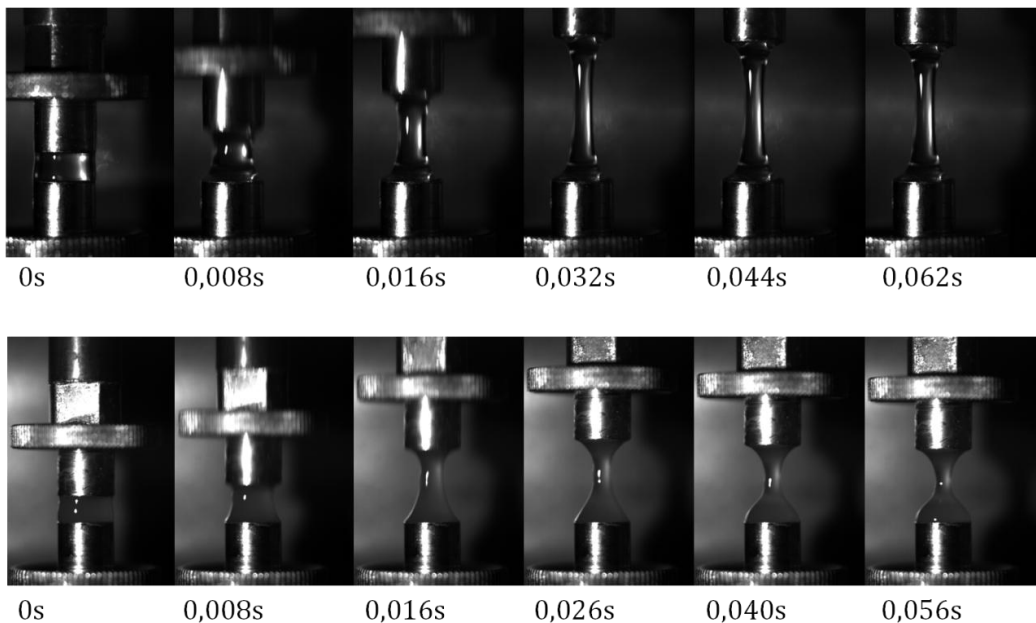

Figure 4.5 Frames extracted from the high speed video during the plate separation stage, approximately at constant time intervals: the series above refers to S8000 sample, while the second to C225 fluid

The midplane diameter values were evaluated with ImageJ software and then, for each test, they were plotted in a log-log scale plot to verify whether the slope was actually equal to $-\frac{3}{4}$; an example of the interpolation operation is shown in Graph 4.1.

Equation	y = a + b*x		
Weight	No Weighting		
Residual Sum of Squares	2,68993E-4		
Pearson's r	-0,99884		
Adj. R-Square	0,9971		
		Value	Standard Error
Log (R/Ro)	Intercept	8,92104E-4	0,00679
	Slope	-0,74286	0,01793

Graph 4.1 Interpolation of the six diameter values extracted by the image processing with Spiegelberg equation (4.1)
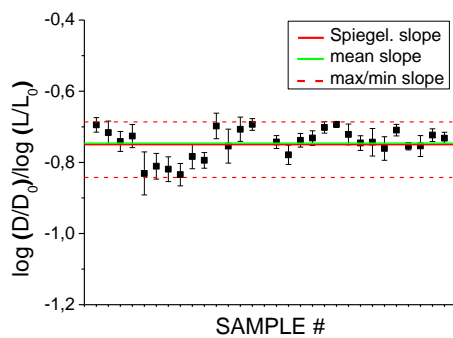
Graph 4.2 Evaluated slopes for the S8000 samples with reference to Spiegelberg equation one
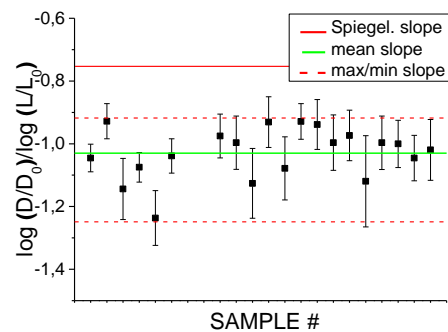
Graph 4.3 Evaluated slopes for the C225 samples with reference to Spiegelberg equation one

The results of the interpolations showed that the Spiegelberg's prediction was consistent with the data obtained from the tests on S8000 (Graph 4.2), but definitely not with the C225 ones (Graph 4.3). Therefore, this approach is not suitable for system with complex rheological behaviour, and it was not considered to be adequate for the solutions object of the present work.

After this attempts, it became evident that a reliable value for D^* could be evaluated only from video image processing. As a consequence, all the CaBER tests on Nylon6 - $FeCl_3 \cdot 6H_2O$ solutions were recorded with the high speed camera available, using 500 fps frame rate (frame size: 1000x1000 pixel) and Computar Macro 10X lens. This choice, though, required the tests to be performed with the sample chamber open, otherwise no video would have been taken.

It is worth observing that from the high speed video it is also possible to obtain some qualitative information about the evolution of the liquid thread, which can be essential for the interpretation of the solution behaviour and the extraction of the extensional rheological properties. The usefulness of this information is more exhaustively explained in the following section.

4.1.3. Methods for experimental data analysis

The output of a CaBER test is essentially experimental points in a diameter-time space, representing the evolution of the midpoint diameter, as measured by the laser micrometer, during the test.

For the data analysis, first of all D^* was evaluated from the high speed camera video, following the procedure described in the previous section. Then, the quantity $\bar{D}$, defined as:

$$\bar{D}(t) = \frac{D(t)}{D^*}$$

(4.3)

where D is the diameter measured by the micrometer, was calculated. This definition allows setting the test beginning at $\bar{D} = 1$, i.e. when the upper plate had stopped its motion. Furthermore, the diameter normalization over D^* make feasible to compare the evolution curves for different samples deriving from the same solution type. This procedure is actually required by the fact that the evolution of the liquid thread is influenced by the real diameter of the initially loaded column (D_0), which obviously will not be exactly the same for all the tests. Thence, rescaling all the curves in terms of $\bar{D}$ allows to get rid of the operator systematic error on solution loading. Similarly, also the times were divided by D^* and they were subtracted by t^*, the time value corresponding to D^*, so as to define a quantity (eq. 4.4) referred to as 'intrinsic time' in this work, which dimensionally is the inverse of a velocity and for which the test beginning was found at $\bar{t} = 0$.

$$\bar{t} = \frac{t - t^*}{D^*}$$

(4.4)

Hereafter, an example of the aforementioned operations is shown: it can be noticed how the two diameter evolution curves, which look significantly different in Graph 4.4 , are

instead much more similar (Graph 4.5), as it emerged when the quantities are reported as defined in equations 4.3 and 4.4.
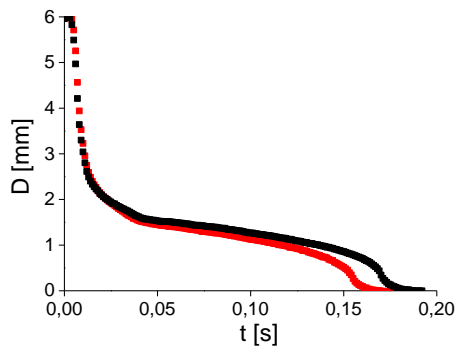
**Graph 4.4 Diameter evolution curves of two 5,5% samples: real measured diameter and time**
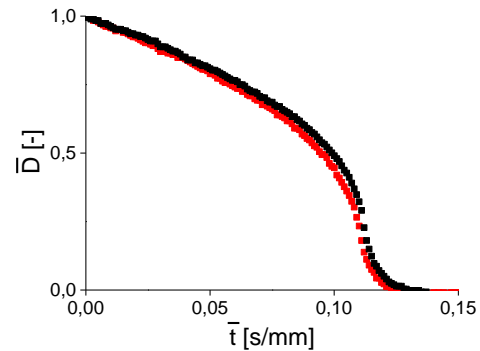
Graph 4.5 Diameter evolution curves of two 5,5% samples: modified diameter (4.3) and time (4.4)

Once the evolution curves had been reported in the more convenient way, the desired quantities could be extracted from the CaBER curves, as explained below.

t_C, intrinsic time to breakup

For all the solution, irrespective of the rheological behaviour, the intrinsic time to breakup was evaluated. The definition 'intrinsic time' comes from the fact that this quantity, thanks to its definition, is independent of the CaBER test parameters, although actually it does not have the dimension of a time. Provided D^* is the same for all the samples, $\overline{t}_C$ gives a rough idea on the effect of capillary and viscoelastic forces, being higher when the second ones are larger. In this case, the solution is expected to form stable threads. However, as already discussed, the kinetics of the diameter evolution is affected by actual value of D^*, which is not always the same, neither for different samples of the same solution, thus looking at the true time can deceiving, while $\overline{t}$ should be unaffected by D^*. Then, $\overline{t}_C$ was defined as the value of $\overline{t}$ at which the normalized diameter $\overline{D}$ equals zero; an example is shown in Graph 4.6. Thanks to this definition, it follows that $\overline{t}_C$ does not depend on CaBER test parameters, but it is a function only of the material properties, so it can be referred to as 'intrinsic time', though considering that it does not actually have the dimension of a time.
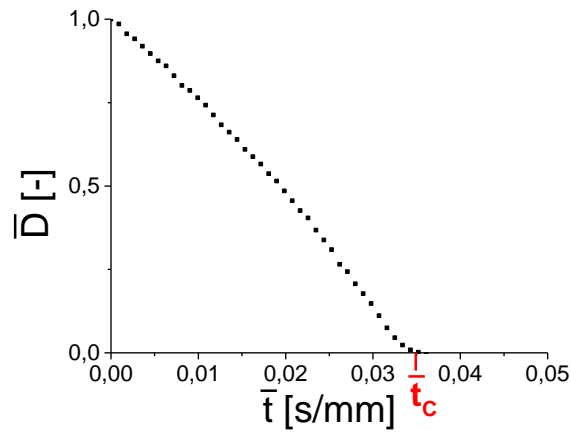
Graph 4.6 Example of the evaluation of t_c for a 3,5% FeCl$_3$ sample

λ_C, polymer characteristic relaxation time

The characteristic relaxation times were evaluated on the basis of the analysis proposed by Entov and Hinch (Entov, et al., 1997), discussed in detail in chapter 2. Here, it is essential to recall that, when a viscoelastic liquid is subjected to capillary thinning, at a certain stage the elastic stress are grown enough to become dominant and the strain rate drops, leading to a slow down of the thinning process. At this stage, the dynamics with which the filament diameter evolves is described as:

$$D_{mid}(t) = D^* \left(\frac{D^* G}{4\sigma} \right)^{\frac{1}{3}} \exp\left(-\frac{t}{3\lambda_c} \right) \tag{4.5}$$

where σ is the surface tension, G a shear elastic modulus, λ_C the characteristic relaxation time.

In a semi logarithmic plot, equation 4.5 describes a linear dependence of the diameter with respect to time, and the slope results to be inversely proportional to the characteristic relaxation λ_C.

$$\ln D(t) = \ln K - \frac{1}{3\lambda_C} t \tag{4.6}$$

Hence, if the solution behaviour had been identified as viscoelastic (E), the diameter curves were plotted in a semi log scale and its linear part at intermediate times was fitted with an equation of the type: $y = mx + q$ (see Graph 4.7).
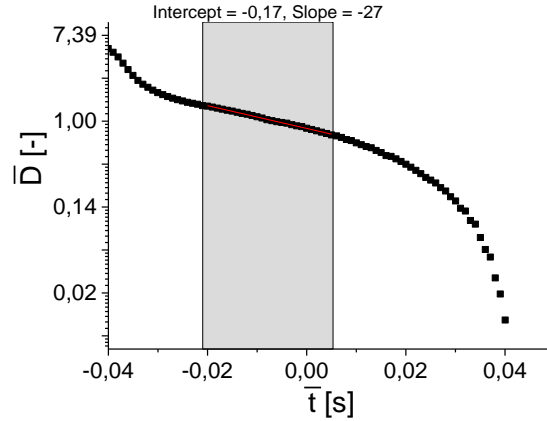
Graph 4.7 Example of diameter evolution curve linear interpolation for a 3,5% FeCl₃ sample

From the obtained value of the slope, m, λ_C was calculated as:

$$\lambda_C = -\frac{1}{3m} \qquad (4.7)$$

v_C, capillary velocity

The capillary velocity is defined as the ratio between surface tension and shear viscosity:

$$v_C = \frac{\sigma}{\eta} \qquad (4.8)$$

and represents the relative effect of capillary and viscous force. From CaBER tests, it can be measured at later stages of the thread thinning process, when the gravitational drainage effect is negligible and, for a polymeric fluid, in the limit of finite extension of the macromolecular chains, when the elastic stress fully relaxes (Entov, et al., 1997). In the present analysis, following the McKinley and Tripathi approach (McKinley, et al., 2000), the Bond number (eq.4.9), was taken as representative of the relative effects of gravity and capillarity.

$$Bo = \frac{\rho g D^2}{4\sigma} \qquad (4.9)$$

with σ surface tension, ρ fluid density, g gravity and D filament diameter.

When this ratio is low enough (in this work the limit was set at $Bo = 0,07$) and provided no elastic forces acts on the thread, its diameter decreases linearly with time, as

$$D_{mid}(t) = D* - C\frac{\sigma}{\eta}t \qquad (4.10)$$

with σ surface tension, η fluid viscosity and C empirical constant. Thus, from the slope of this curve, v_C can be determined.

It should be observed that v_C can be also predicted from independent measurement of surface tension and shear viscosity. Therefore, this quantity can be used to estimate the reliability and accuracy of the measurements by comparing the results deriving from different testing techniques.

Determination of solution behaviour

In order to be able to extract the information from the measurements in a correct way, it is necessary to choose the constitutive behaviour consistent with experimental observations. As already mentioned in chapter 2, the D^* evolution curve shows a different features for a viscous fluid and a viscoelastic one. Indeed, while for the former the shape is theoretically expected to turn downwardly after a first straight stage, for the latter it turns upwardly, as sketched in Figure 4.6.
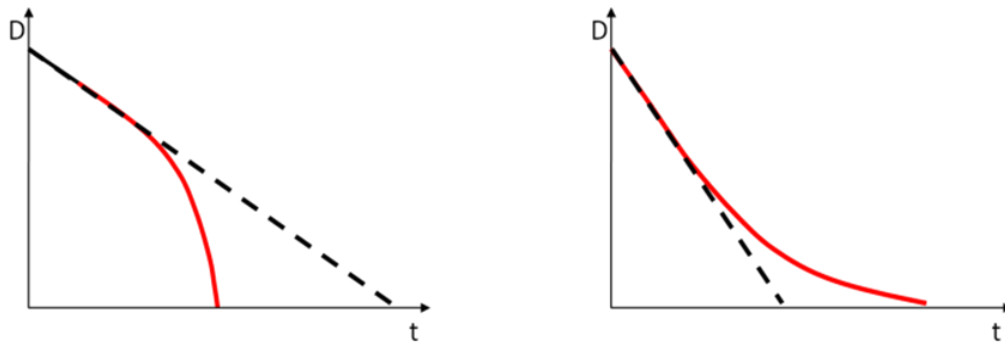
Figure 4.6 Sketches of theoretically expected shapes for a viscoelastic fluid (left) and a viscous one (right). The dot line is just a visual aid to highlight respectively the upward or downward turn of the curves

Though theory gives a very clear indication on how to choose the constitutive behaviour, in practice it is not always so straightforward to distinguish whether the behaviour is viscous or viscoelastic, especially when dealing with complex fluids, as in the present case. In such systems, the behaviour is often in the midstream of the previous two.

A helpful method to overcome this issue was identified during the study, based on the observation of both the midplane diameter evolution curve, from the laser micrometer, and the shape of the whole filament, from the video recordings. This followed from the fact that also shape of the evolving liquid thread is quite different (Figure 4.7), depending on the nature of the fluid (see chapter 2).
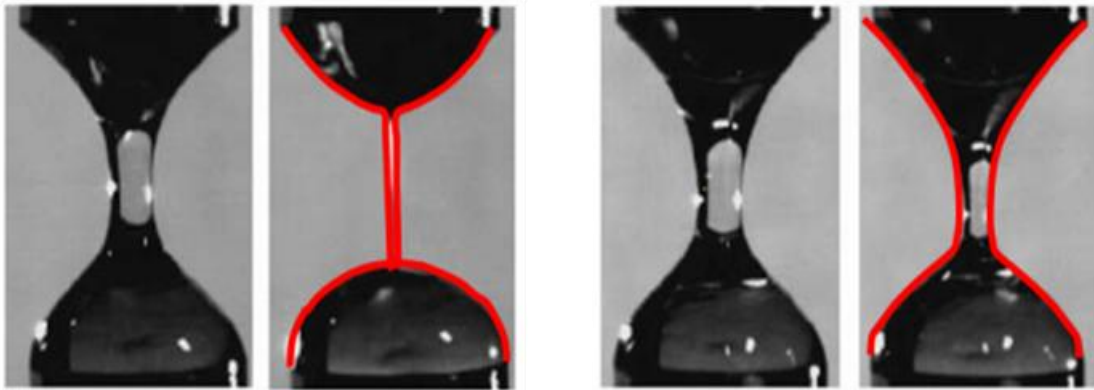
Figure 4.7 Shapes of evolving threads of model liquids: a viscoelastic fluid (left) and a viscous one (right). The red lines are just to highlight the differences in the neck extension and shape

Therefore, the distinction between viscous (V) and viscoelastic (E) solution was performed by looking both at the shapes of the evolution curves and of the evolving liquid filament and then by comparing them. When the behaviour could not be ascribed with any doubt to these two categories, it was defined as intermediate (V/E).

4.2. Electrospun fibre production and characterization

4.2.1. Electrospinning experimental apparatus

As far as the electrospinning technique is concerned, the process was performed with the support of the same research group, already mentioned in the case of the solution preparation.

Specifically, the process was carried out at room temperature, with a vertical configuration and a bottom to top spinning direction.

The feeding solution was loaded in a 2,5 mL syringe with a 22 gauge needle (Hamilton Gaslight model 1002 TLL). The syringe was later positioned on an infusion pump (KDS Scientific, model series 200) which fed the polymer solution into the capillary nozzle at a constant flow rate, fixed at 0,07 mL/h.

A high voltage power supply (Spellman SL30P300) was connected to the needle to provide the driving potential, which was set at 15 kV.

An adjustable grounded stand was used to support the upper stainless steel plate (collector), which was positioned at 20 cm from the nozzle, such that the fibres formed were dry when they hit the collector. Both glass and silicon substrates were positioned on the plate in order to collect the fibre webs.

4.2.2. Fibre web characterization

Morphological analysis

The morphological analysis of the fibres was performed both through an optical microscope (Optika) and a Scanning Electron Microscope ((FEG) LEO 1525).

The analysis with the optical microscope was made on the fibres collected on glass substrates and it was carried out immediately after the spinning process, in order to have a first glance and to verify if the fibre formation had effectively occurred.

The SEM analysis was performed on silicon substrates to investigate the fibre morphology in a more accurate and detailed way. Images were taken at different magnification, ranging from 10 kX to 140 kX, depending on the morphology. As an example, Figure 4.8

shows sample SEM images at different magnifications for the fibres obtained with the 5,6% solution.
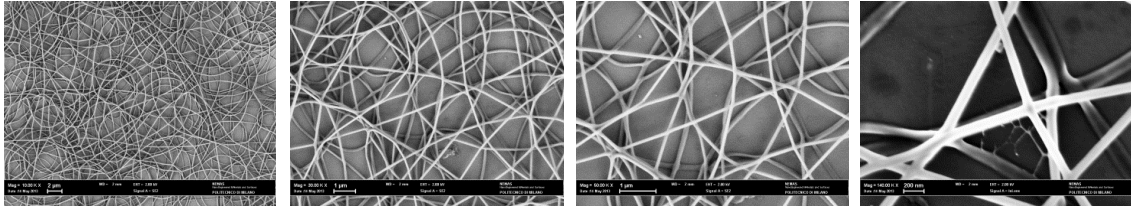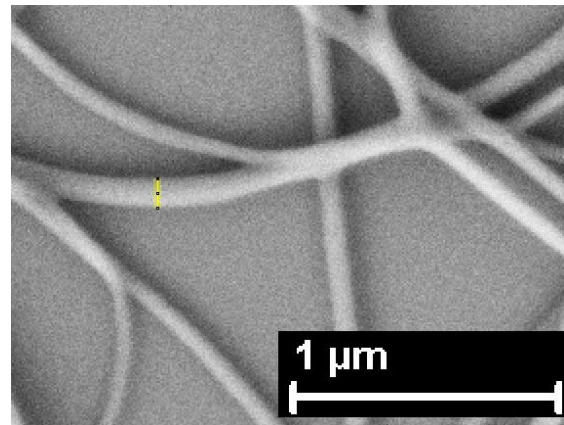

Figure 4.8 SEM images at different magnifications for the fibres obtained with the 5,6% FeCl$_3$ solution; moving left to right: 10kX, 30kX, 50kX, 140kX

At a later stage, the diameter distribution and the mean diameter size were determined from the SEM images using an image processing software (ImageJ). For each solution, the diameters were measured from different 50 kX images, as shown in Figure 4.9 and Figure 4.10, obtaining in total about 60 values per electrospun solution type. These results were then used to determine the diameter distribution and the mean diameter size. In some cases, where fibre branching had occurred, the study of the distribution suggested the presence of two families of fibre diameters (Figure 4.11), a bigger and a smaller one, the specific dimensions depending on branching and solution type. In these instances, only smaller diameter family was considered for the measurements.
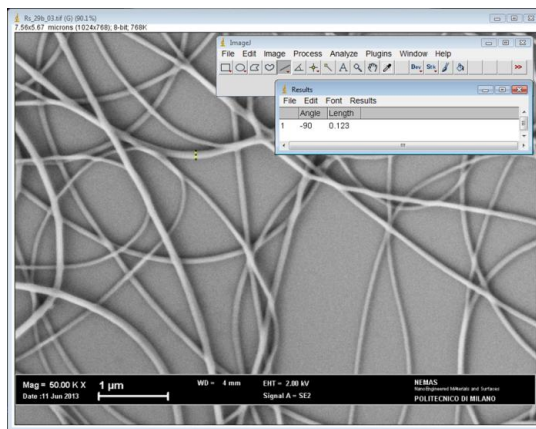
Figure 4.9 Example of the diameter measuring operation with ImageJ software

Figure 4.10 Magnification of figure 1.9: the yellow line is the segment considered for the diameter evaluation
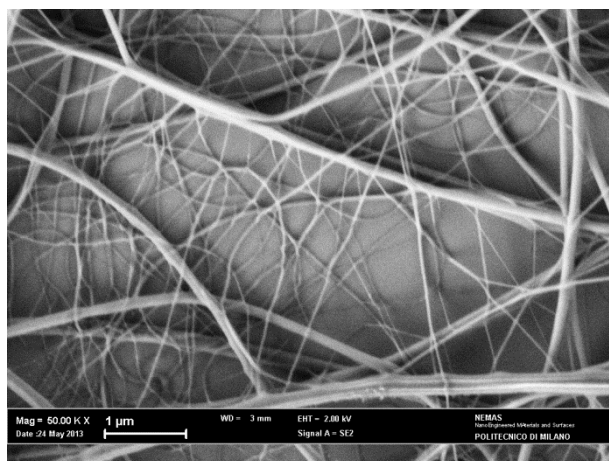
Figure 4.11 Example of a SEM image for a branched fibre morphology (1,5% FeCl$_3$)

Thermal analysis

Differential Scanning Calorimetry (DSC) was used to obtain information about the cristallinity of the electrospun fibres. After the web had been recovered by scratching from the glass substrate, the fibres were placed in 40 μl aluminium crucibles (Me-27331, Mettler) and weighted with an analytical balance (Mettler AE163).

The thermal scan was performed with Mettler DSC-30 connected to a Mettler Toledo TC15 TA controller. All the samples underwent a thermal history constituted by a first heating ramp from 25°C to 100°C at a 5°C/min rate, a cooling ramp from 100°C to 25°C at 5°C/min, an two-minute isothermal step at 25°C and a second heating ramp from 25°C to 250°C at 5°C/min. A sketch of the thermal history is shown in Graph 4.8.
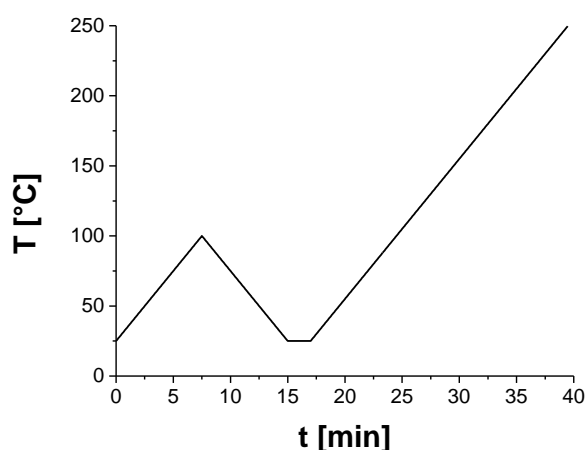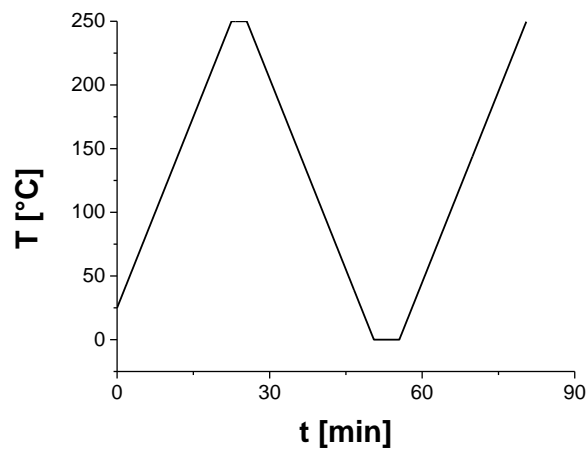

Graph 4.8 Sketch of dsc thermal history

For every scan, a 50 ml/min nitrogen flux was set through the DSC camera, in order to remove the gasses that may have been developed during the measurements. The crucibles were weighted a second time after the thermal scan had been performed, so as to verify if any mass loss took place.

The melting temperature and enthalpy were evaluated with STARe software from heat flow-temperature plots. It is worth noting that the heat flow was normalized with respect to the sample fibres mass and that only the second heating ramp scan was taken into account, as the first one was performed only to remove the water that could have been absorbed by the fibres after the spinning process.

A thermal scan was carried out also on PA6 pellets, in order to have a reference scan diagram for the unprocessed material. In this case, the sample was subjected to the thermal history displayed in Graph 4.9, where the first heating ramp, from 25°C to 250°C at 5°C/min, was applied to completely remove the effect of possible previous heat treatments, while the two-minute isothermal steps at 250°C and 0°C were carried out to remove the measurement noise. Similarly to what was done for the fibre samples, only the second heating ramp was analyzed for the thermal characterization of the pellets.

Graph 4.9 Sketch of DSC thermal history for PA6 pellet

4.3. Solution characterization

Some of the solutions were also characterized with other techniques, in order to extract, in addition to the elongational rheological properties, useful measures of surface tension, density and shear viscosity, necessary to estimate the adimensional numbers presented in chapter 2.

Surface tension measurements were performed with a video-based optical contact angle measuring system (DataPhysics OCA 15EC). The evaluation was done for five solutions (0%, 1%, 4,5%, 5,6%, 6,5%) through the pendant drop method and for each sample at least three measures were executed.

Due to the lack of a suitable amount of solution, no conventional technique could be used and the density was simply evaluated by weighting a known volume of solution (2 mL) with an analytical balance (Mettler AE163). The measures was performed on five solutions (0%, 1%, 4,5%, 5,6%, 6,5%), as it was done for surface tension measurements.

Shear viscosity measurements were performed with a DRS 200 Rheometrics rotational rheometer. A plate-plate geometry was used and the gap varied between 0,5-0,7 mm. As the iron(III) chloride hexahydrate solutions are highly corrosive, disposable 40 mm aluminium plates were used during the tests. The scansions were carried out at 30°C, imposing a linear stress ramp from 0 to 500 Pa in 3 minutes and acquiring 200 points per decade. As previously specified for surface tension and density, only five solutions (0%, 1%, 4,5%, 5,6%, 6,5%) were tested. For every solution type, the evaluations were performed on two different samples, each one scanned twice, in order to verify the repeatability of the measures. Anyhow, it is necessary to report that the solutions at high iron chloride content (4,5%, 5,6%, 6,5%) noticeably underwent some kind of alteration during the tests. This is likely to have been an effect of both plate corrosion and water absorption from the environment, as no humidity control was enforced during the tests. This said, these phenomena may probably be the cause of the problems arisen from the shear viscosity measurements (as the non-repeatability of the test on the same sample and so on), and thus they should be taken into account for the purpose of the result analysis in chapter 5

Results and discussion

The aim of the present chapter is to present the experimental results obtained according to the methods described in the previous chapter. After some paragraphs concerning the outcomes of a specific testing or analysis technique, a further interpretation of the experimental results, based on the theoretical background proposed in chapter 2, is discussed in detail in section 5.4.

5.1. CaBER results

Above all else, in this first section the results concerning the elongational rheological characterization are discussed.
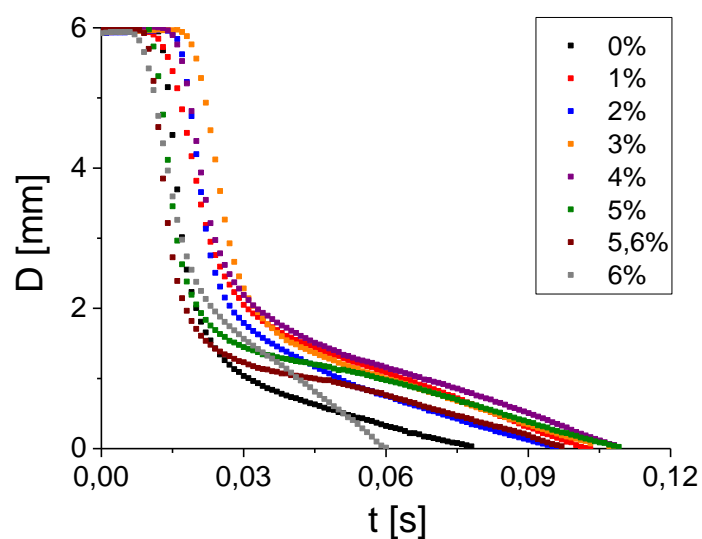
Graph 5.1 Diameter evolution curves of some solutions of the systematic study (one sample for solution type)

Graph 5.1 represents the very rough outcome of a CaBER test, that is the evolution of the thread middle diameter as measured by the laser micrometer; in this particular case, some examples for different $FeCl_3$ contents are shown. First of all, it has to be noticed that the measures result to have been performed at the very limit of the instrument resolution, as the fluids were characterized by a very fast diameter evolution if compared to simpler model liquids. Nevertheless, at a first sight, the shape of the curve seems to be consistent with the typical one for viscoelastic fluids, with the exception of the 6,5% solution, which appears quiet different from the other ones. This said, it was decided to extract the characteristic polymer relaxation times (λ_c) from these measurements, employing the Entov-Hinch approach shown in chapter 4, extending the method also to 6,5% solution, whose analysis has to be carried out carefully. The results are represented in Graph 5.2 as a function of iron chloride content. The λ_c values are found to be almost constant until 3,5%, then a slight increase occurs in correspondence of midway solutions behaviours, and finally it drops to very lower value at 6,5%.
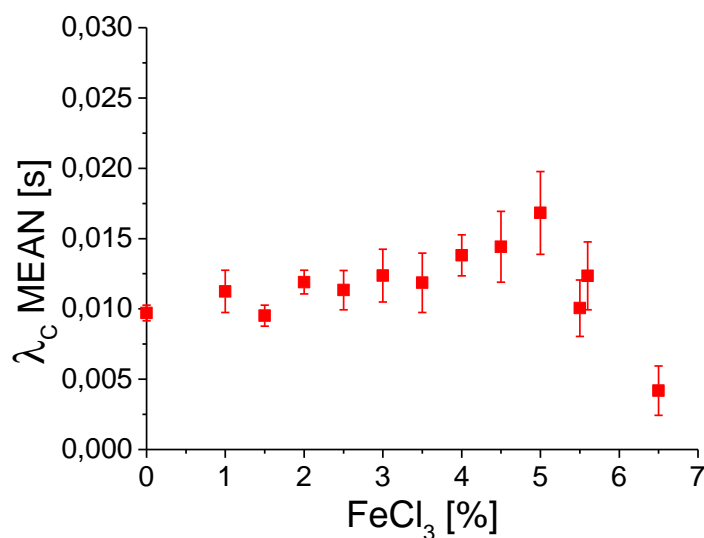
**Graph 5.2 Polymer relaxation time as a function of the FeCl₃ content**

Except for the drop observed at high concentrations, these results are not consistent with the theoretically expected trend: as formerly mentioned, an increase in the $FeCl_3$ content is supposed to limit the H-bond presence between amide groups, thus reducing the solution elasticity and so the relaxation time. Here, up to 3,5% the solution behaviour seems not to be affected by the progressive increase in the salt content, or at least not in a sufficiently evident way. The further increase of the evaluated λ_c is absolutely in contrast with the theoretical prediction and apparently meaningless. In light of these considerations, it was

thought that the presence of the iron chloride may induce some kind of transition in the solution behaviour above a certain threshold. This might imply a progressive unsuitableness of the Entov-Hinch model, actually applicable for dilute viscoelastic fluids, as the $FeCl_3$ content increase. A first proof may be shown by the gradual broadening of the standard error associated to the evaluation of the λ_c mean value.

A rough discrimination of the solution behaviour can be directly gathered from the evaluation of the intrinsic time to breakup $\bar{t}_c$ from the CaBER diameter evolution curves. In fact, as already mentioned in chapter 4, this quantity provides an approximate idea on the solution viscoelasticity, being higher when the degree of elasticity is higher. Thereby, $\bar{t}_c$ was estimated from the $\bar{D}$ vs. $\bar{t}$ curves (examples are plotted in Graph 5.3) for all the solutions; Graph 5.4 shows the data points corresponding to the breakup event for the different samples of the same solution.
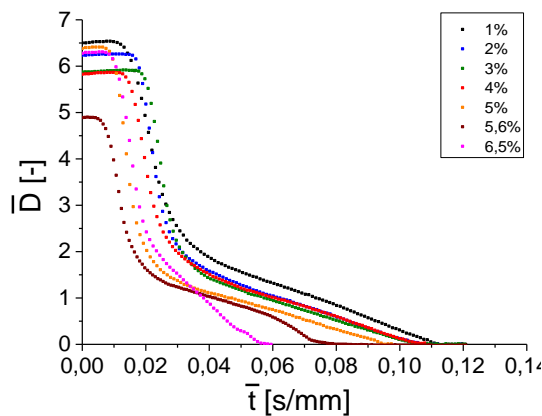
Graph 5.3 Diameter evolution curves of all the solutions of the systematic study (one sample for solution type)
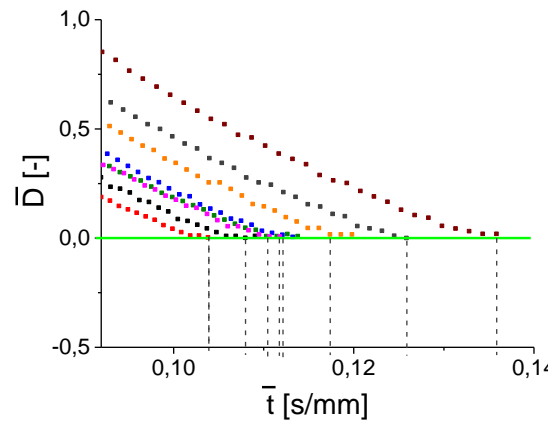
Graph 5.4 Data points corresponding to the breakup event for the different samples of the 1,5% FeCl₃ solution

In Graph 5.5 all the mean $\bar{t}_c$ values are represented with respect to the iron salt content: as it can be noticed, at increasing $FeCl_3$ content they remain almost constant up to 4%, after which a drop in $\bar{t}_c$ is observed. It has to be pointed out that the value corresponding at 5,5% is not coherent with the other solution trend, and thus need further investigations. However, if this point is excluded from the analysis, the trend showed in Graph 5.5 is consistent with the theoretical prediction discussed in chapter 4, as the $\bar{t}_c$ drop at high salt content reveals the progressive fading of solution viscoelasticity.
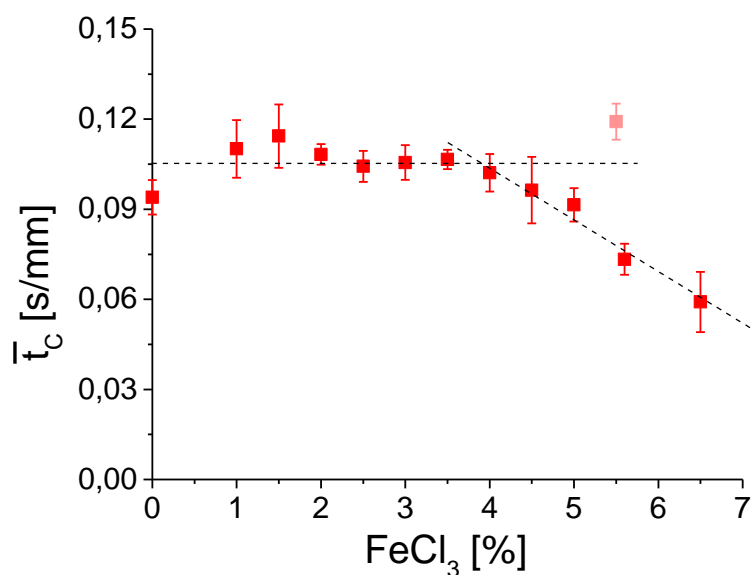
Graph 5.5 Mean $\bar{t}_C$ values represented as a function of the FeCl₃ content: the dashed lines are just a visual aid and do not represent any fitting

From the previous comments, it was enlightened that the evaluation of $\bar{t}_C$ allowed to get a rough idea of the solution viscoelasticity. A more accurate distinction between viscous (V) and viscoelastic (E) solutions was then performed by looking both at $\bar{D}(\bar{t})$ curves shapes and the shape of the thread, as already illustrated in chapter 4. It has to be noticed that, when the thread behaviour could not be ascribed with any doubt to one of these two categories, it was defined as intermediate (V/E). As far as these rheological considerations are concerned, it has actually been all but easy to identify the most appropriate constitutive behaviour, since complex dilute systems, such the one considered in this work, are characterized by very slight different features. As an example, the Graph 5.6 and Graph 5.7 represent the evolution curves obtained for the samples of two different solutions, the first identified as viscoelastic (E) and the second as a midway/viscous one (V/E). Similarly, some frames of the relevant high speed video recordings in Figure 5.1 and Figure 5.2. All the $\bar{D}(\bar{t})$ curves obtained from CaBER measurements are reported in Annex A.
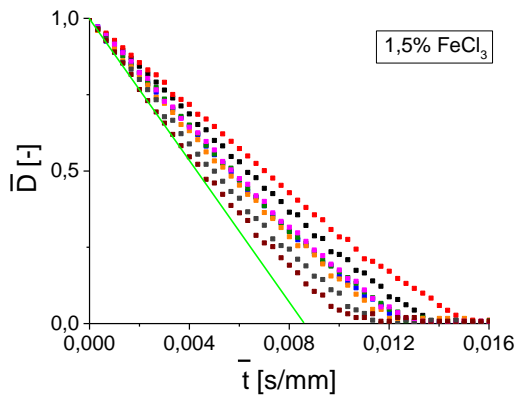
Graph 5.6 Evolution curves for 1,5% FeCl₃ solution samples (green line is just a visual aid to identify the upward turn)
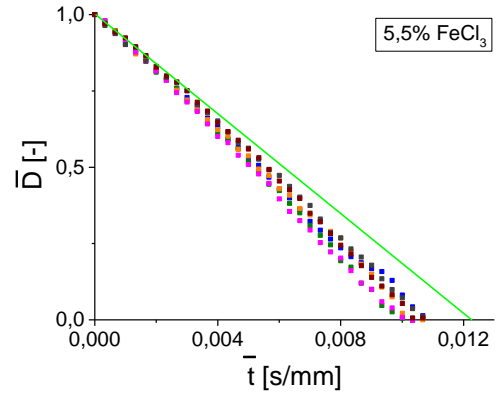
Graph 5.7 evolution curves for 5,5% FeCl₃ solution samples (green line is just a visual aid to identify the downward turn)
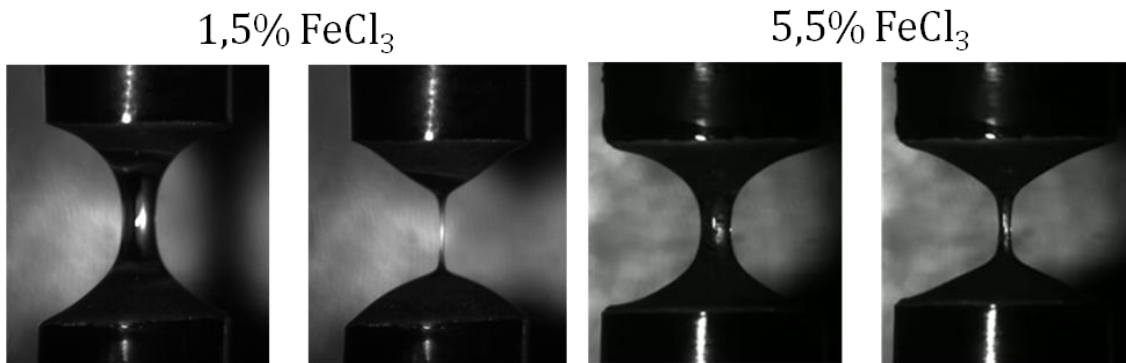
$$1,5\% \text{ FeCl}_3 \qquad 5,5\% \text{ FeCl}_3$$

Figure 5.1 Frames from high speed video of the caber test on a 1,5% FeCl₃ sample

Figure 5.2 Frames from high speed video of the caber test on a 5,5% FeCl₃ sample

From the previous images it is possible to observe that, although the previous graphs and figures exhibit the peculiar features of a viscoelastic response, both in terms of upward turn in the $\bar{D}(\bar{t})$ curve and extended homogeneous thread, the differences among the two samples are not so straightforward at a first glance, as it was instead shown in chapter 4 for simpler model fluids.

The results of the analysis are reported as a function of FeCl₃ content in Graph 5.8, from which it is possible to point out about three main regions. In the first, from 0% up to 3%, the solution behaviour is clearly identified as viscoelastic, both from video and CaBER curve observations; by gradually increasing the content of the iron chloride, a transition region, in which the fluids are behaving midway between E and V, is encountered. Finally, at high FeCl₃ content the behaviour moves towards the viscous one, as particularly clear from $\bar{D}(\bar{t})$ plots, until no more elasticity is observed at 6,5% with no doubt from both the observations. These results are consistent with the theoretical effect of FeCl₃ and the

previous considerations concerning $\bar{t}_c$, since they confirm that the effect of an increasing salt content is to induce a transition, though not so sharp, in the solution behaviour, by gradually reducing system viscoelasticity until a completely viscous behaviour is observed.
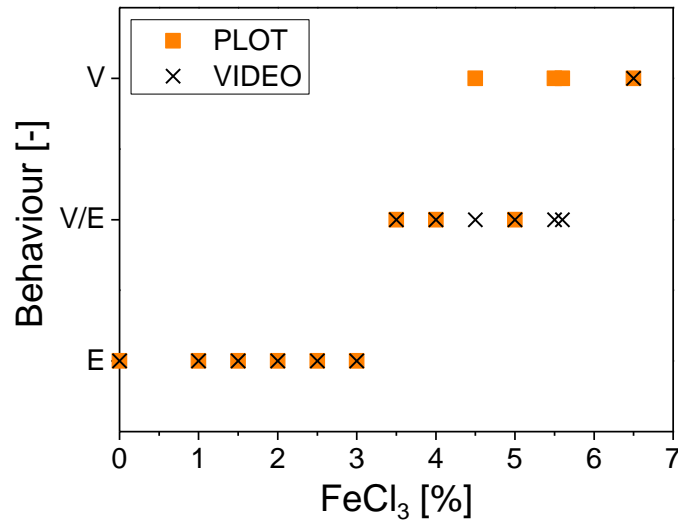
Graph 5.8 Rheological behaviour of the solutions from D(t) curves/video comparison

It is worth noting that estimating λ_c for midway and viscous behaviour is not in principle appropriate, nevertheless it can be still useful to highlight a transition in the solution behaviour, in this specific case from a viscoelastic to a viscous response. Oddly, the transition results in an apparent increase in λ_c when going from E to V/E behaviour and the expected drop when the viscosity dominates the flow. This trend is hard to explain, nonetheless it suggests the polymer relaxation times evaluated for high salt content (pink-coloured in Graph 5.9) are to be employed very carefully for further data manipulation.
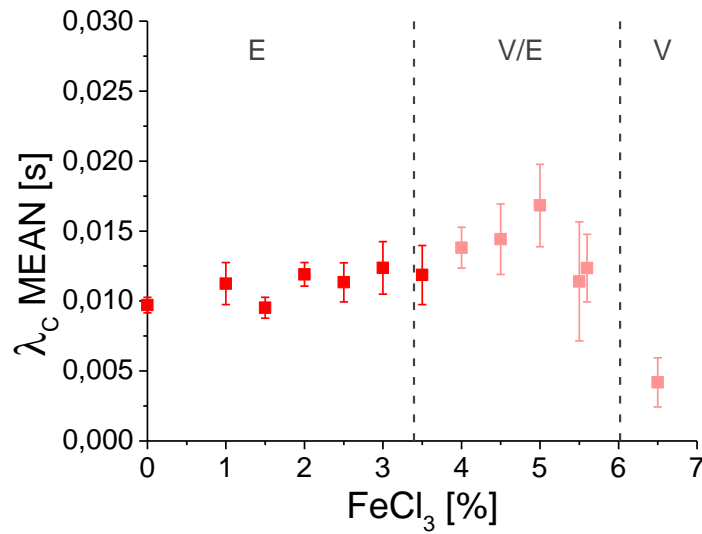
Graph 5.9 Polymer relaxation time as a function of the FeCl₃ content

# 5.2. Solution characterization results

Although they are not essential to the purpose of this work, it has been considered worthwhile to disclose the results obtained from the other solution characterization tests, since they will be helpful for the further interpretation of the spinning output.

The results obtained from the density measuments are shown in Graph 5.10. As it can be noticed, the densities are almost constant for the considered solutions, having a mean value equals to $1,23 \pm 0,01 \ g\big/cm^3$. It has to be observed that the mean solution density is approximately the same of the formic acid one ($1,22 \ g\big/cm^3$).

The same constant trend is followed by the surface tension, as all solutions are in a narrow range around the mean value $39,51 \ mN/m$. Although the effect of Nylon 6 was to slightly increase the surface tension, since the solvent itself is characterized by $\sigma = 37,84 \ mN/m$, the mean value is quiet low for a polymeric solution, which leads to the beneficial effect of contrasting Rayleigh instability during the electrospinning process, as mentioned in chapter 1.
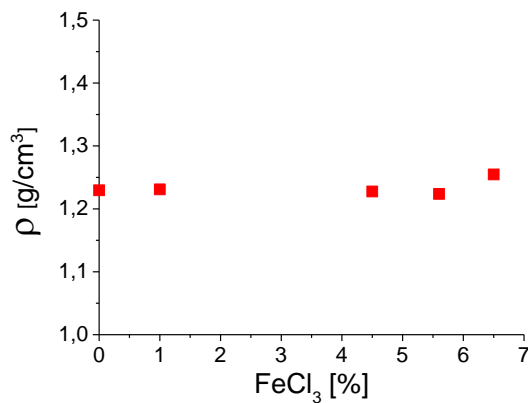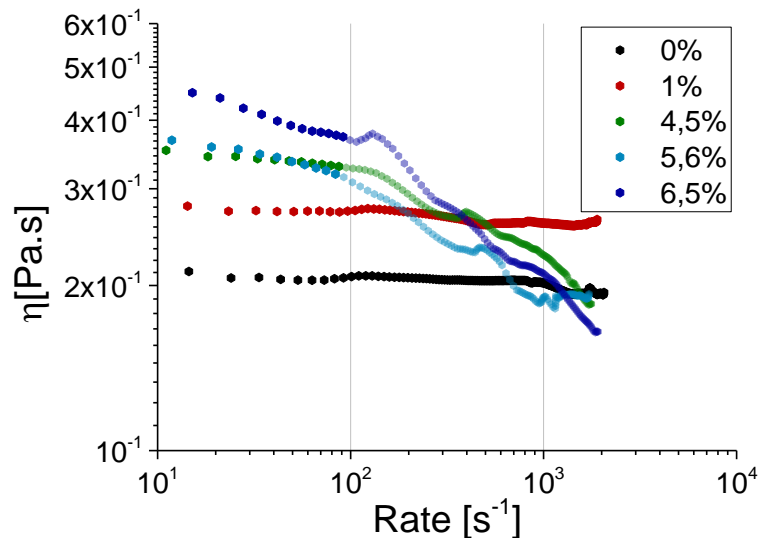
Graph 5.10 Solution density as a function of the FeCl₃ content
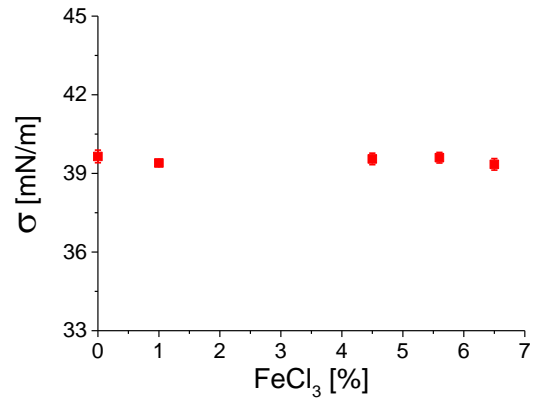
Graph 5.11 Solution density as a function of the FeCl₃ content

Graph 5.12 shows the measured shear viscosity versus shear rate for the five tested solutions. From these results, it seems that, at different salt concentrations, two different behaviours are present.


**Graph 5.12 Shear viscosity measurements versus shear rate for the five tested solutions**

At low FeCl₃ contents, the solutions behave like Newtonian fluids, with shear viscosities being independent on the shear rate in the investigated range. Nevertheless, from the CaBER measurements the 0% and 1% solutions was definitely found to be viscoelastic. This difference, that at a glance looks nonsense, is instead typical of the so-called Boger fluids, which are elastic liquids with a constant, or nearly so, shear viscosity (James, 2009). Otherwise, at high FeCl₃ contents, the shear behaviour appears to be non-Newtonian, as

the viscosity decreases with the shear rate after a short initial plateau, which anyway is completely flat only for the 4,5% solution. Moreover, on these solutions the results were not repeatable, since the second scans on 4,5%, 5,6% and 6,5% samples were found to be completely different from the first ones. In chapter 4 it was already anticipated that some issues were encountered during this test progressions, because both plate corrosion and water absorption from the environment are supposed to have been occurring and they may be the cause of the odd features arisen from the shear measurements.

Due to the huge extent of problems during the shear measurements, the approach of the capillary velocity mentioned in chapter 4 was employed to verify the reliability and accuracy of these results. For the shear viscosity evaluation, in light of the above considerations, it was decided not to consider the whole curves for the three aforementioned concentrations, but only the first part (in details up to $7 \cdot 10^{-1} \ s^{-1}$), and to estimate the shear viscosity from a regression performed on this section. On the other hand, in order to extract v_C from CaBER tests, the Bond number was set equal to $0,07$, so as to estimate a critical thread diameter size D_{cr} after which the gravity effects are negligible. Then, a linear interpolation of the diameter evolution curves was performed after D_{cr} (Graph 5.13), and v_C was evaluated using equation 4.10. Comparing the results gained from the different techniques, it can be noticed that they are consistent (see Graph 5.14). Thereby, the shear viscosity measures can be supposed to be reasonably reliable.
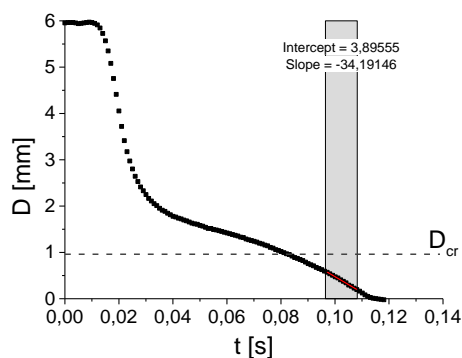
Graph 5.13 Example of the linear interpolation of D(t) curve after D_cr for extracting v_c
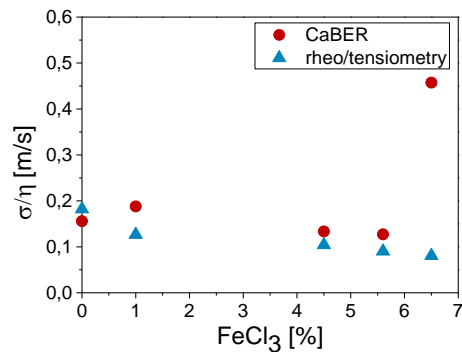
Graph 5.14 Comparison of the capillary velocity values evaluated from caber test and rheo/tensiometry measures
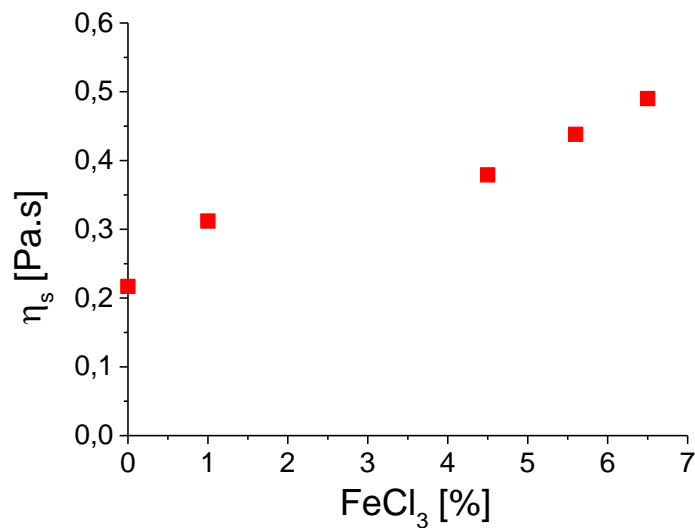
Graph 5.15 Evaluated solution viscosity as a function of the FeCl$_3$ content

Once the reliability of the shear measures has been assessed, limiting the analysis to the part of the curve unaffected by solution alterations, it is possible to observe that the higher is the content of FeCl$_3$, the higher is the shear viscosity (Graph 5.15). This result might be explained hypothesizing that the macromolecular coils are swollen because of the steric hindrance of the hexahydrate chloride molecules. Under shear, this could lead to an effect similar to the one caused by raising the polymer molecular weight, that is a viscosity increase due to the enhancement of coil interactions. This observation appears again to be in contrast with respect to what was stated so far on the basis of the extensional measures; however, it has to be borne in mind that shear and elongation implies in truth different mechanism of chain deformation. The before-written hypothesis is not necessarily true also for elongation, in which it actually seems that the predominant effect of the salt is the reduction of chain interactions due to formation of complexes with amide groups and H-bond scission. Anyway, the real effect of iron salt on the macromolecular chains, and thus on different flow types, needs to be further investigated.

Another interesting observation arising from these measures is the outward contradiction among shear viscosity increase and $\bar{t}_C$ decrease with salt content. As a matter of facts, the latter quantity depends on the overall evolution of the thread, which at different times is controlled by different properties. Only if all of them, except one, are held constant, the effect of this one can be singled out. This may be the case of pure PA6 and 1% FeCl$_3$ solution, which are expected to have similar relaxation times and show a small increase in $\bar{t}_C$, which might depend on the viscosity trend. For the other concentrations, the

concurrent changes in elastic and viscous properties affects $\overline{t}_C$ in a difficult to interpret way. Nonetheless, when viscous effects become dominant for any kind of fluid that is just before the break up the system response is coherent with shear viscosity measurements, as already demonstrated by the comparison in **Graph 5.14**.

5.3. Electrospun fibre characterization

5.3.1. SEM images analysis

From the SEM images shown in Figure 5.3, the fibre morphologies at different $FeCl_3$concentrations can be observed. Images at different magnification are reported in Annex B. As a general remark, all the fibrous membranes are characterized by an almost uniform morphology, until 6,5% content is reached: at this critical concentration, it is impossible to identify a real fibre formation any more, but just fibre traces with segregated polymer/salt particles. In some cases the occurrence of branches can be noticed, especially at low concentrations: at without salt, the formation of quite large fibres occurred, together with very thin secondary ones; conversely, at 1,5% in particular, small uniform fibres coexist with larger secondary structure. For two specific solutions, namely 4,5% and 5%, some solvent spots were observed on the silicon substrates: this observation is not consistent with the uniform dried membranes obtained from 2% up to 5,6%, but it may be ascribed to the effect of slightly different ambient conditions during the process, in particular to an higher relative humidity in the lab environment.
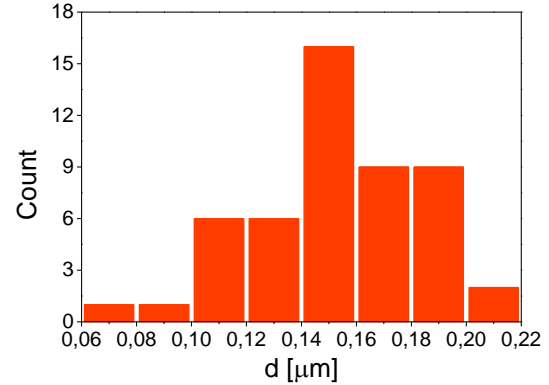

0%   1%   1,5%   2%

2,5%   3%   3,5%   4%

4,5%   5%   5,5%   5,6%   6,5%
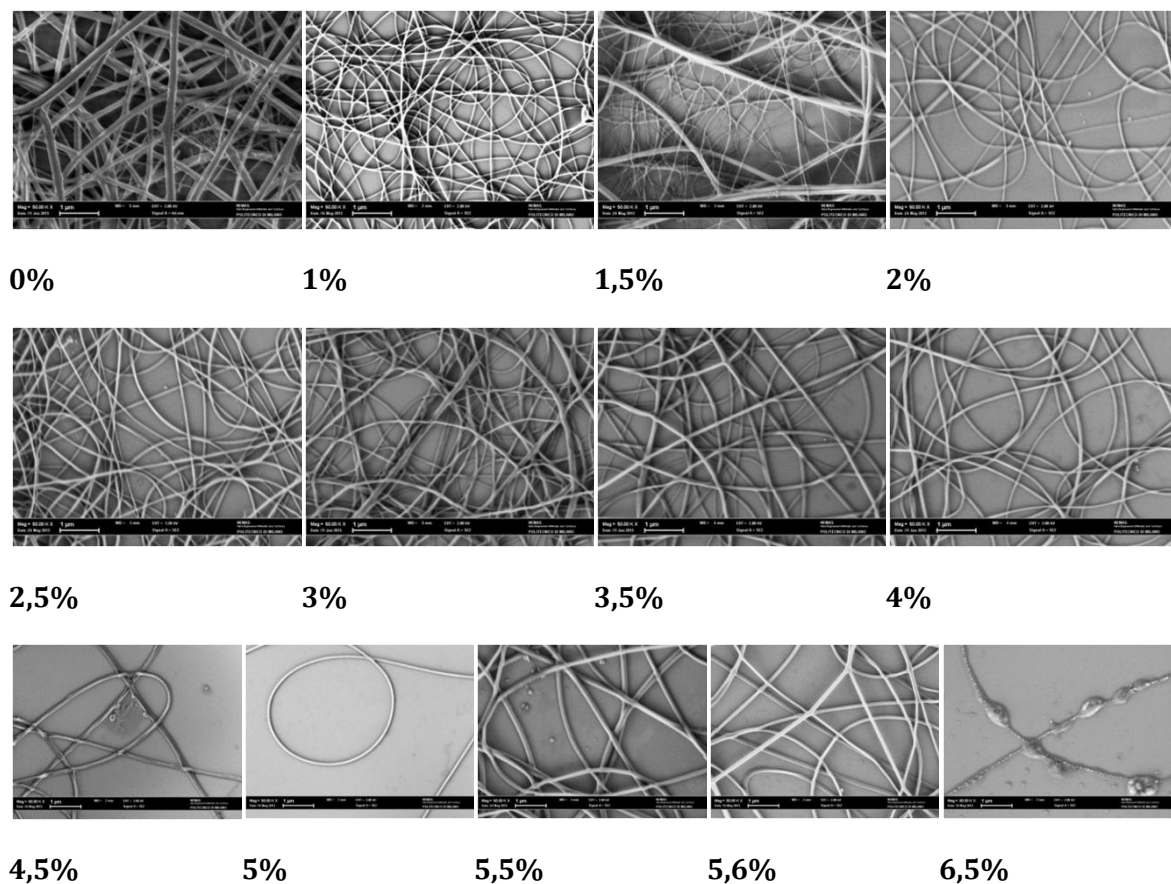
**Figure 5.3 Examples of SEM images for the solutions at the different FeCl$_3$ content**
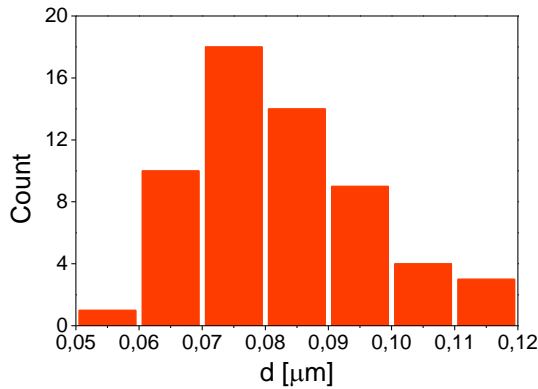
Graph 5.16 Diameters frequency distribution for the solution at 3% FeCl₃ content

Graph 5.17 Diameters frequency distribution for the solution at 5,6% FeCl₃ content

The analysis of the fibre diameter distribution showed a Gaussian statistic trend for about all the solutions (see Graph 5.16 and Graph 5.17), with the exception of the low content branched membranes, in which a bimodal distribution is observed. As already mentioned, in these instances the evaluation of the mean diameter size, $\overline{d}$, was performed on the base of the smaller diameter family. It was also observed that the higher the content of the ionic salt content, the less scattered the diameter distribution, as reported also in the work of Cai et al. (Cai, et al., 2011) mentioned in chapter 1.

In Graph 5.18 the mean diameter value is plotted with respect to the FeCl₃ concentration. As it can be observed, a slight increase in the FeCl₃ content caused a remarkable drop of $\overline{d}$: from 0% to 1% the fibre diameter was actually reduced by more than four times. This experimental observation can be easily explained considering that the addition of the ionic salt causes a dramatic increase of the solution electrical conductivity, allowing for a greater jet elongation during its flight towards the collector. As the FeCl₃ gradually increased, a progressive increase of $\overline{d}$ was found. The observed increase in the shear viscosity for high FeCl₃ content can account for this trend, which at a first sight seems quiet unexpected, considering that the solution conductivity is supposed to be rather enhanced by gradually increasing the salt content (Cai, et al., 2011). However, it has to be noticed that the mean diameter size at 5,6%, which is the higher concentration at which fibres were formed, is still about three quarter the one of pure Nylon6 fibres.
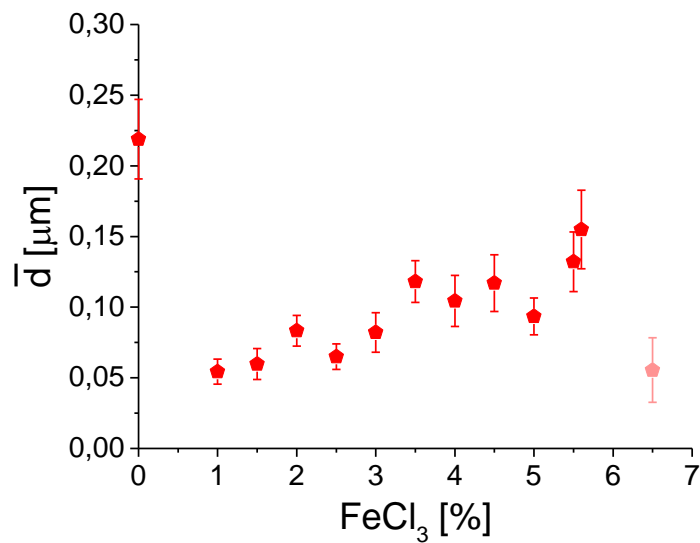
Graph 5.18 Mean diameter size as function of FeCl₃ content

If the aim of this specific fibrous web is called to mind, that is to be employed as template for PANI in situ polymerization, it is clear that an appropriate balance between a high content of ionic salt and fibre uniformity have to be searched for. That being so, the analysis of the fibre SEM images actually pointed out that the best condition is found for the 5,6% FeCl₃ solution, as it combines a high salt content with a branching-free uniform morphology and also a smaller diameter size if compared to the pure Nylon6 one. This result is in agreement with a previous work, where iron(III)chloride anhydrous was used instead of the hexahydrate one and interestingly the same concentration was chosen from the optimization of the spinning process.

5.3.2.   DSC thermogram analysis

The results of the thermal analysis performed on the electrospun webs are shown in Graph 5.19. Since the purpose of DSC measures was to evaluate the cristallinity of the fibres after the spinning process, only the second heating scan was taken into account. First of all, as it can be observed from Graph 5.19, it is impossible to identify any glass transition, although undoubtedly the polymer is supposed to contain an amorphous phase. However, this can be easily explained considering that the samples were in very low quantities (less than a mg, though usually some mg are used), so the noise of the measurement may have cloaked the transition. On the other hand, it is possible to identify a melting peak in each thermogram up to 4,5% $FeCl_3$, meaning that the electrospun fibres produced from solutions with concentration above that results to be completely amorphous, as it is confirmed by the lack of an endothermic peak in the 5,6% scan.
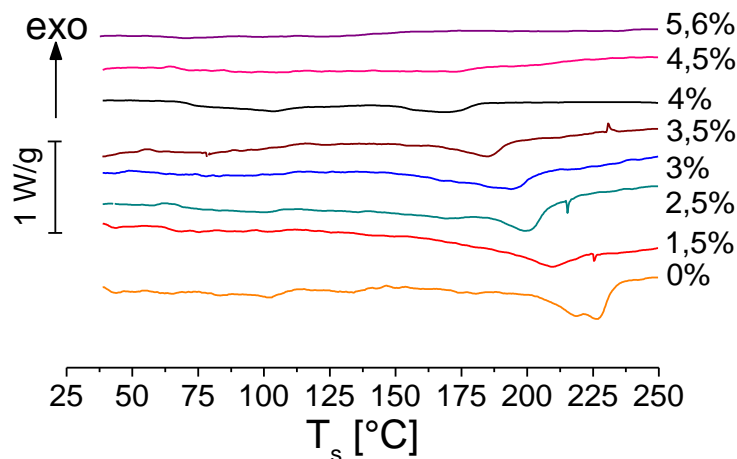
Graph 5.19 DSC thermograms for all the tested solutions

Furthermore, it can be noticed that the melting peaks are always very broad, which is a sign of the scattered distribution of the size of the crystals. If the scan of the pure Nylon6 electrospun fibres is compared to the one of the Nylon6 pellets, the unprocessed material shows a narrower and higher endothermic peak (Graph 5.20), which indicates that the material had a crystalline phase made of very similar and ordered structures before the spinning process. In addition, literature survey shows that electrospinning changes the chain conformation of Nylon6: Raman spectroscopy was exploited to investigate the structure of the polymer before and after the process, and it resulted that there was a

change in the backbone structure, which can be related not to the degradation of the PA6, but rather to the transformation of the bulk conformation, α-form, to the γ-form (Stephens, et al., 2004).
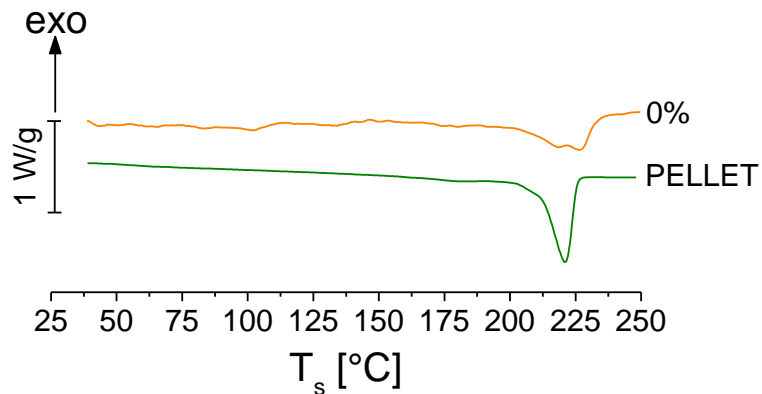

Graph 5.20 Comparison of the DSC thermograms of the PA6 pellets and the 15% PA6 solution without salt

It is worth noting that the thermal analysis provided some interesting results concerning the amount and the perfection of the crystals. Observing the scans in Graph 5.19, it immediately stands out that somewhat trend exist between the amount of $FeCl_3$ in solution and the extent and position of the peaks. Indeed, at first sight it seems that increasing the content of $FeCl_3$ entails progressively smaller peaks at ever lower temperature that means less perfect crystals. Quantitative validations of these observations were get considering the melting enthalpies (peak area) and temperatures (peak position) of the fibres: Graph 5.21 shows that the higher is the iron chloride content, the lower is the melting enthalpy, while Graph 5.22 exhibits again a decreasing trend for both the melting temperature and the temperature of melting onset at increasing salt content. This said, it is evident that $FeCl_3$ does have an effect on fibres cristallinity, as far as its presence seems to disturb the formation of crystal phase during the spinning process.
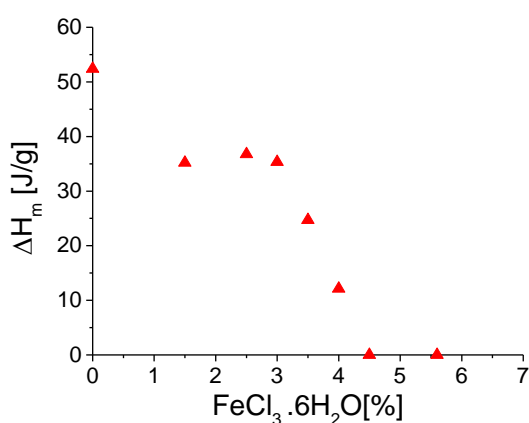
Graph 5.21 Melting enthalpy as a function of the FeCl₃ content
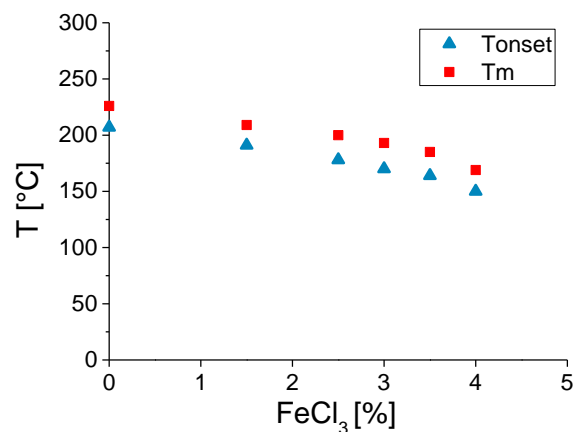
Graph 5.22 Melting onset temperature (triangle) and melting temperature (square) as a function of the FeCl₃ content

An interpretation of these results can be given in the wake of several literature papers that report studies about the effect of inorganic salt on bulk properties of different polymers (Cai, et al., 2011)(Starkweather Jr, et al., 1993). In particular, Valenti et al (Valenti, et al., 1973) showed that the rate of crystallization and the melting temperature of synthetic Nylon4 and Nylon6 were both decreased by adding an ever larger amount of LiCl, due to the site-specific hydrogen bonds scission and the formation of salt-polymer complexes. Moreover, they noticed that there exists a limiting concentration, beyond which enough amide groups are complexed so that no crystallization is possible any further. The same effect was found by Kim and Harget (Kim, et al., 1979), who observed that salts lowered the melting temperature independently of their type and the crystallization conditions. In the present work, the worsening and decrease of cristallinity at increasing $FeCl_3$ content, up to the critical concentration of 4,5%, above which no crystallization of Nylon6 occurred, is very similar to the literature trends. Thereby, these effects can be ascribed to the formation of amide-salt complexes that prevents H-bonds and disturbs the polymer crystallization under stretching during the jet flight towards the collector.

A further interesting correlation was observed between the rheological behaviour of the solutions and the cristallinity of the electrospun fibres. Indeed, the cristallinity was completely lost almost as soon as it starts becoming impossible to discriminate the solution behaviour, or better when the viscoelasticity is sufficiently reduced by the presence of the ionic salt (Graph 5.23). Nevertheless, it seems that the cristallinity is not essentially controlled by the elongational rheology, although certainly influenced by it, but rather by the steric hindrance of the salt, since the same transition was observed in crystallization in quiescent conditions(Valenti, et al., 1973)(Cai, et al., 2011).
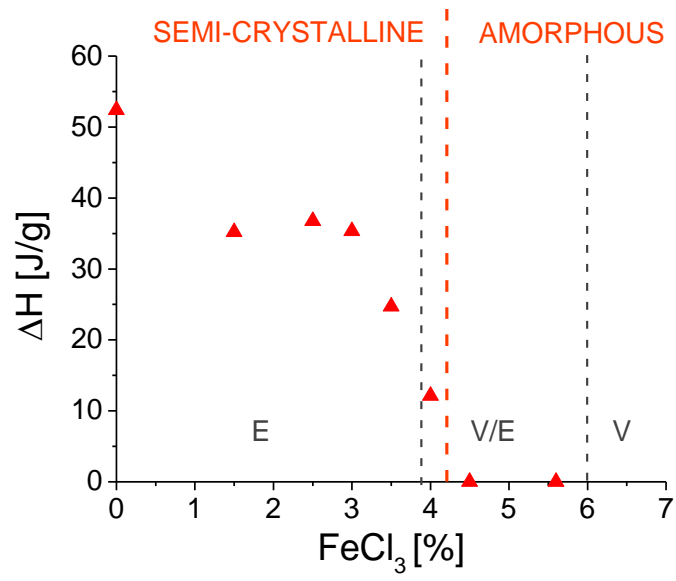
Graph 5.23 Comparison between melting enthalpies, crystalline structure and rheological behaviours

5.4. Adimensional analysis and result correlations

The complexity concerning the interpretation of the experimental results obtained from the CaBER measurements has been highlighted in the previous sections. Indeed, understanding the constitutive rheological behaviour of the system object of this study proved to be quiet tricky, since in some cases it was impossible to discriminate whether the solution was showing a viscoelastic, or a simply viscous, response. What is more, the criterion chosen to identify the more appropriate behaviour of a sample, though based on a suitable theoretical background, is not so objective as sought, as it is largely based on the operator judgement and interpretation. Hence, it arose the urgency to seek a different criterion that could lead to clearer evidence about the dominant rheological effects in the considered flow. To this end, the tool of adimensional analysis represents an effective answer, as it allows implementing an approach less subject to the scientist judgement. Moreover, this method should in principle help not only to establish whether or not a solution is viscoelastic, but also to effectively relate the rheological behaviour to the heuristic and poorly quantified concept of 'spinnability'. Thereby, the adimensional quantities defined in chapter 2 - Elastocapillary, Deborah and Ohnesorge numbers - were evaluated for the solutions of this methodical study.

To check the robustness of the approach, data from CaBER measurements were analyzed as if the fluid behaviour was viscoelastic, with no a priori check about this hypothesis. The Ec number was then calculated, though this was done only for the five solutions on which the tensiometry and shear rheology measures were available. The obtained values are shown in Graph 5.24 with respect to the iron chloride content and, as it can be observed, the Ec number decreases as the salt percentage increases, with the exception of the 1% content, showing a value lower than that of the general trend. However, the important information to be extracted is if Ec is above or below unity, as, Ec greater than one means that the flow is dominated by the fluid elasticity (see chapter 2). This is the case of $FeCl_3$ contents up to 5,6%. Conversely, Ec is less than unity for the 6,5% solution, indicating that in this case the timescale for viscous phenomena is longer than the relaxation time. All these results not only are in good agreement with $\bar{D}(\bar{t})$ evolution analysis and direct observation of the thread, but also clarify the solution behaviour in that range between 4% and 5,6%, where no univocal interpretations could be given on the basis of the CaBER measurements. In light of these considerations, it can thus be concluded that the approach based on Ec evaluation is valid.
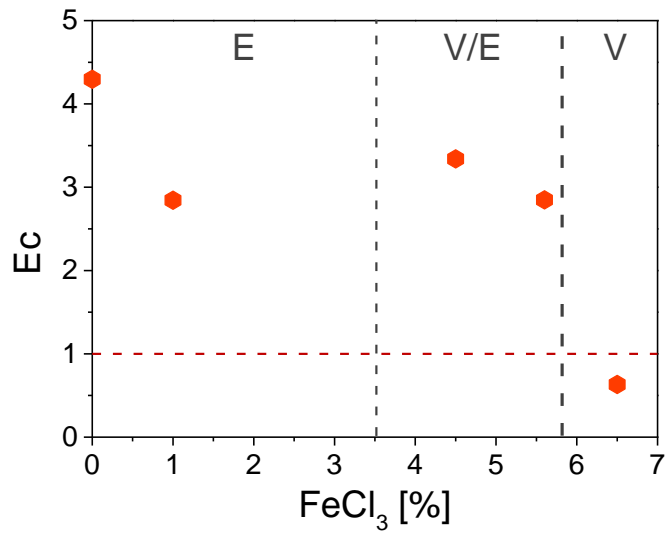
Graph 5.24 Estimated Elastocapillary number (Ec) as a function of the FeCl₃ content

Besides allowing assessing the rheological behaviour of the different solutions, the Elastocapillary number was used to identify the effect of the iron chloride content on the solution spinnability. Indeed, the necessary condition for a fluid to be electrospun is to have a certain degree of elasticity, or better the flow has to be elastically dominated, in order to allow the jet stretching and elongation during the electrospinning. Accordingly, considering the outcome of the spinning process, it appears that fibre formation occurs for all the solution except for the 6,5% one, that is, as expected, the only fluid characterized by $Ec < 1$, and hence by a viscous dominated response (Graph 5.25).
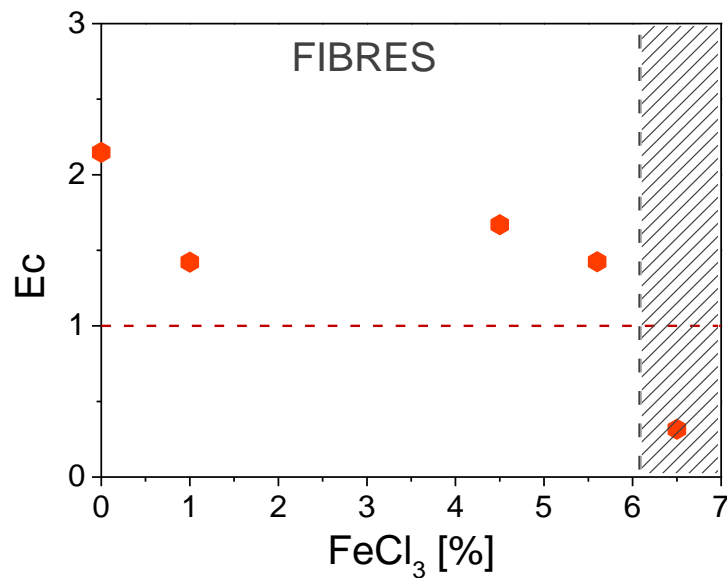
Graph 5.25 Comparison between the elastocapillary number values and the electrospinning outcome: dashed zone corresponds to unspinnability region

At this point, the effect of the ionic salt on the solution viscoelasticity has been evaluated. Then, the influence of the salt content should be reflected also by the presence of defects in the electrospun fibres, as, according to literature survey, the latter is mainly influenced by the extensional rheological properties of the feed solution. This can be verified considering the adimensional Deborah number, since it allows to verify if elastic stresses relaxes slowly enough to arrest Rayleigh instability ($De > 1$), thus avoiding electrospraying but not 'beads-on-a-string' defects, or even to prevent it ($De \gg 1$), favouring the formation of uniform fibres. In the present case, the evaluation of De shows a slightly increasing trend as the content of the iron chloride approaches 5,6%, then a drastic drop corresponding to the solution at 6,5% (Graph 5.26). Defect-free fibres were obtained for all the elastically stabilized solutions (with $De \geq 6$), while at 6,5%, when De is very near to unity, instability occurred and almost no fibres formed.

Again, the good agreement between the results of adimensional analysis and the outcomes of electrospinning suggest that the approach exploited is valid and this seems true even if the meaning of λ_C is somehow questionable in light of the intermediate (V/E) behaviour of the solution during capillary breakup. In order to shed some more light on this, it would have been interesting to investigate solution with $1 \leq De < 6$ and checking if the expected beaded morphologies were obtained. Unluckily, the considered system changes quiet abruptly between 5,6% and 6,5% and no defect-rich morphology could be got. A further study with more controllable solutions should be required to confirm the above observations.

Finally, it's interesting to notice that $De > 6$ is the same result as reported by Yu et al. (Yu, et al., 2006) in their work on PEG-PEO aqueous solutions. This is however fortuitous, as in the present work De was determined taking correctly into account the length scale typical of Rayleigh instability in the CaBER measurement; however, since the length scale of the electrospinning is smaller, the values of De are expected to be higher for the same solutions in that process.
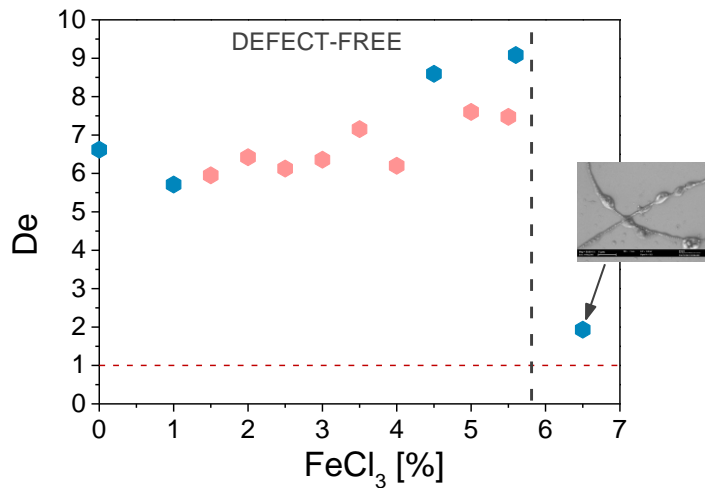
Graph 5.26 Comparison between the Deborah number (De) values and the electrospinning outcome as a function of the FeCl$_3$ content

Considering finally the Ohnesorge number, it can be convenient to show the results of the adimensional analysis in the operating diagram proposed by McKinley (McKinley, 2005) (see chapter 2). As it can be observed (Graph 5.27), the viscoelastic solutions (0%, 1%, 4,5%, 5,6%) are located in the upper half-plane and have both De and Oh greater than unity, which are the optimal operating conditions for the electrospinning process ad defined by McKinley (see Figure 5.4). Consistently, these solutions revealed spinnable and allowed the production of homogeneous fibres. Instead, the unspinnable viscous solution (6,5%) is, as expected, in the viscous dominated region at a relatively high Ohnesorge number. The impossibility of spinning this solution, despite the high Oh value, is a further evidence of the preeminent relevance of the elongational properties with respect to the shear ones in determining the process feasibility and outcome. Basically, no matter how viscous a solution is, if it does not have a sufficient degree of elasticity.
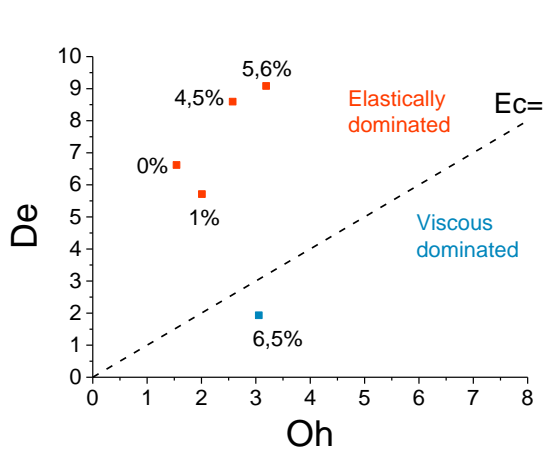
Graph 5.27 Tested solutions in the two space operating diagram
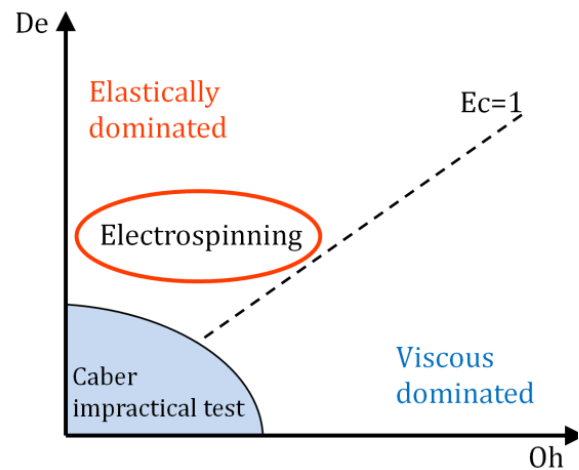
Figure 5.4 Adimensional space diagram with the operating area for the electrospinning process

The above considerations about the Elastocapillary and Deborah numbers have demonstrated the expected effect of the ionic salt on decreasing the viscoelastic character of the solutions. It is noteworthy how the transition from viscoelastic to completely viscous behaviour, determined from the capillary breakup phenomenon and Ec number, occurs at exactly the same iron chloride content at which the transition from spinnability to unspinnability and from uniformity to almost absence of fibres are observed from the outcomes of electrospinning process.

Concerning remarks

The aim of the present work was to check the possibility to exploit the phenomenon of viscoelasto-capillary thinning and breakup to investigate the rheological behaviour of a fluid and predict its (electro)spinnability. Accordingly, the attention was focused on a solution on PA6 and iron(III) chloride hexahydrate in formic acid and a systematic study was carried out at varying salt concentration in order to identify the effects of this variable on the solutions rheological behaviour and on the morphology of the fibres electrospun from it.

The SEM observations of the latter demonstrated the formation of homogeneous fibres up to a $FeCl_3$ concentration of 5,6%, while at 6,5% a significantly non-homogeneous "beads-on-string" structure – and maybe also isolated beads, produced by electrospraying rather than electrospinning – is observed.

The results of the rheological characterization of the same solutions, carried out both by traditional shear rheometry and by capillary breakup extensional rheometry, showed that the addition of $FeCl_3$ to the PA6 solution increases the shear viscosity, probably due to the fact that the macromolecular coils are swollen because of the steric hindrance of $FeCl_3$ and hence the interactions among them are enhanced. Simultaneously, it lowers solution elasticity due to the hydrogen bond scission, induced by the formation of complexes between the salt and the amide groups of the PA6 backbones. Moreover, two regimes, a first, at lower $FeCl_3$ concentrations, in which a clear viscoelastic behaviour could be observed, and a second, at higher salt concentration, characterized by a response closer to a viscous one, could be made out. Several clues are available to back this observation, such as the transition in the dependence on $FeCl_3$ content of time to rupture and in the apparent relaxation times, or the change in the shape of the diameter evolution curve in CaBER experiments, or yet the change in the shape of the flow curve in shear. Nevertheless, the

different observations could hardly be put together and correlated with those from electrospinning, and they were even contradictory to some extent.

An effective synthesis and interpretation of all the experimental observations was made possible resorting to adimensional analysis, which allowed evaluating the relative contribution to the flow of viscoelastic stress relaxation, viscous flow and surface tension action during capillary breakup. As this kind of flow occurs in absence of any external force, three adimensional number were taken into consideration: the Elastocapillary number, Ec, the Deborah number, De, and the Ohnesorge number, Oh, in agreement with the theoretical works by McKinley (). As the capillary breakup phenomenon was considered, a proper length scale was set, corresponding to thread diameter at the end of stretching phase.

Following this approach it was found that Ec keeps higher than unity and slightly decreases with increasing $FeCl_3$ content up to a concentration of 5,6% and then drops to a value less than unity for 6,5%. The trend confirms the effect of ionic salt in lowering the elasticity of the solution by shielding the inter-chains interaction. Further, the drop to Ec<1 for the 6,5% solution confirms that only at this concentration the solution behaves like a viscous fluid during capillary breakup. The adimensional analysis seems thus a valuable tool to investigate the constitutive behaviour of a fluid during capillary breakup, even if it should be noticed that only the change to fully viscous behaviour could be detected by the analysis, which didn't allow detecting the transition at intermediate times, apparent if intrinsic time to breakup of relaxation times are considered.

As for correlation with electrospinning, the drop in Ec correlates with the defects observed in ill-formed fibres when 6,5% $FeCl_3$ solution is electrospun, as, according to McKinley (McKinley, 2005) Ec>1, is a necessary condition for spinnability. Also the De dependence on $FeCl_3$ content show a very good agreement with the outcomes of electrospinning: in detail De is about 6 for all the concentration except 6,5%, where De≅1. Accordingly, fibres spun for all solutions but the 6,5% show uniform diameter, while the latter results ill-formed and highly defective.

It can be thus concluded that the capillary breakup rheometry is a powerful technique to investigate the viscoelastic/viscous behaviour of solutions, and that adimensional analysis can be exploited both to investigate the capillary breakup phenomenon – at least to some extent - and to predict the behaviour of solutions during electrospinning. It also worthwhile notice that it is true even in case – as the present – in which characterization is quite challenging both due to chemical instability and to its low viscosity and fast relaxation phenomena in the solutions.

From a process analysis standpoint, the suitability of the technique follows from the capability of emphasizing solutions the elastic behaviour which turns out to be the controlling property in the formation of fibres and stabilization of forming thread.

Besides the effect on the rheological behaviour and fibre morphology, the $FeCl_3$ content was shown to affect also the electrospun fibre cristallinity, as above a critical concentration fibres turn out to be completely amorphous. Interestingly, this concentration coincides with the one at which the viscous components starts playing a significant role in the rheological behaviour, which is about 4% $FeCl_3$ content. From a structural point of view, both the phenomenon seems to be due to the steric hindrance of the $FeCl_3$, rather than being correlated to each other.

Bibliography

Anna S.L. e McKinley G.H. Elasto-capillary Thinning and Breakup of Model Elastic Liquids [Rivista] // J. Rheol.. - 2001. - 1 : Vol. 45. - p. 115-138.

Cai Yibing [et al.] Effects of ferric chloride on structure, surface morphology and combustion property of electrospun polyacrylonitrile composite nanofibers [Rivista] // Fibers and Polymers. - [s.l.] : The Korean Fiber Society, 2011. - 1 : Vol. 12. - p. 145-150. - ISSN: 1229-9197 DOI: 10.1007/s12221-011-0145-x.

Casper C. L., Stephens J. S. Tassi N. G. Chase D. B. \& Rabolt J. F. Controlling Surface Morphology of Electrospun Polystyrene Fibers:? Effect of Humidity and Molecular Weight in the Electrospinning Process [Rivista] // Macromolecules. - 2004. - Vol. 37(2). - p. 573-578.

Di'az M. N.J. Pinto, J. Gao e MacDiarmid A. G. National Conference of Undergraduate Research [Atti di convegno] // Electrospinning nanofibers of polyaniline and polyaniline/(polystyrene and polyethylene oxide) blend. - Lexington : [s.n.], 2001.

Entov V.M. e Hinch E.J. Effect of a spectrum of relaxation times on the capillary thinning of a filament of elastic liquid [Rivista] // Journal of Non-Newtonian Fluid Mechanics . - 1997. - 1 : Vol. 72. - p. 31-53. - ISSN: 0377-0257 DOI: http://dx.doi.org/10.1016/S0377-0257(97)00022-0.

Formhals A. US patent 1,975,504 [Rivista]. - 1934. - 1,975,504.

Formhals A. US patent, 2,349,950 [Rivista]. - 1944. - 2,349,950.

Hong Kyung Hwa, Oh Kyung Wha e Kang Tae Jin Preparation of conducting nylon-6 electrospun fiber webs by the in situ polymerization of polyaniline [Rivista] // Journal of Applied Polymer Science. - [s.l.] : Wiley Subscription Services, Inc., A Wiley Company, 2005. - 4 : Vol. 96. - p. 983-991. - ISSN: 1097-4628 DOI: 10.1002/app.21002.

James David F. Boger Fluids [Rivista] // Annual review of fluid mechanics. - 2009. - Vol. 41. - p. 129-142. - ISBN: {978-0-8243-0741-7} ISSN: {0066-4189} DOI: {10.1146/annurev.fluid.010908.165125}.

Kim e Harget Glass transition temperature of nylon 6 Inorganic salt mixtures [Rivista] // Journal of Applied Physics. - 1979. - DOI: 10.1063/1.325796.

Li Fengyu, Zhao Yong e Song Yanlin Core-Shell Nanofibers: Nano Channel and Capsule by Coaxial Electrospinning [Libro] / a cura di Kumar Ashok. - 2010. - Vol. 22. - DOI: DOI: 10.5772/8166.

Liang R.F. Mackley M.R. Rheological characterization of the time and strain dependence for polyisobutylene solutions [Rivista] // Journal of Non-Newtonian Fluid Mechanics. - 1994. - Vol. 01. - DOI: DOI:10.1016/0377-0257(94)85031-3.

Liu H., Kameoka J. Czaplewski D. A. \& Craighead H. G. Polymeric nanowire chemical sensor [Rivista] // Nano Letters. - 2004. - Vol. 4(4). - p. 671-675.

MacDiarmid A. W. Jones, I. Norris J. Gao A. Johnson N. Pinto et al. Synth Met [Rivista]. - 2001. - Vol. 119. - p. 27-30.

McKinley G.H. Dimensionless Groups for Understanding Free Surface Flows of Complex Fluids [Rivista] // Soc. Rheol. Bulletin. - 2005. - Vol. July. - p. 6-9.

McKinley G.H. e Tripathi A. How to Extract the Newtonian Viscosity from Capillary Breakup Measurements in a Filament Rheometer [Rivista] // J. Rheol.. - 2000. - 3 : Vol. 44. - p. 653-670.

McKinley G.H. Visco-elasto-capillary thinning and break-up of complex fluids [Rivista] // HML report. - 2005.

Momentè Roberto A new efficient method to produce defect-free polyaniline nanofibers [Rapporto] : Master's thesis / School of Industrial and Information Engineering. - Politecnico di Milano : [s.n.], 2013.

Nair S. S. Natarajan, S.H. Kim Macromol Rapid Commun [Rivista]. - 2005. - Vol. 26. - p. 1599–1603.

Qi Zhonghua [et al.] Highly porous fibers prepared by electrospinning a ternary system of nonsolvent/solvent/poly(l-lactic acid) [Rivista] // Materials Letters . - 2009. - 3â€"4 : Vol. 63. - p. 415-418. - ISSN: 0167-577X DOI: http://dx.doi.org/10.1016/j.matlet.2008.10.059.

Ramakrishna Seeram [et al.] An Introduction to Electrospinning and Nanofibers [Libro]. - [s.l.] : World Scientific Publishing Company, 2005.

Renardy Michael A numerical study of the asymptotic evolution and breakup of Newtonian and viscoelastic jets [Rivista] // Journal of Non-Newtonian Fluid Mechanics . - 1995. - 2â€"3 : Vol. 59. - p. 267-282. - ISSN: 0377-0257 DOI: http://dx.doi.org/10.1016/0377-0257(95)01375-6.

Reneker D.H. [et al.] Electrospinning of Nanofibers from Polymer Solutions and Melts [Rivista] / a cura di Aref Hassan e van der Giessen Erik. - [s.l.] : Elsevier, 2007. - Vol. 41. - p. 43-346. - ISSN: 0065-2156 DOI: http://dx.doi.org/10.1016/S0065-2156(07)41002-X.

Rodd L.E., Scott T.P.Cooper-White J.J. e McKinley G.H. Capillary Breakup Rheometry of Low-Viscosity Elastic Fluids [Rivista] // Appl. Rheol.. - 2005. - 1 : Vol. 15. - p. 12-27.

Shenoy Suresh L. [et al.] Role of chain entanglements on fiber formation during electrospinning of polymer solutions: good solvent, non-specific polymerâ€"polymer interaction limit [Rivista] // Polymer . - 2005. - 10 : Vol. 46. - p. 3372-3384. - ISSN: 0032-3861 DOI: http://dx.doi.org/10.1016/j.polymer.2005.03.011.

Spiegelberg Stephen H., Ables David C. e McKinley Gareth H. The role of end-effects on measurements of extensional viscosity in filament stretching rheometers [Rivista] // Journal of Non-Newtonian Fluid Mechanics . - 1996. - 2–3 : Vol. 64. - p. 229-267. - ISSN: 0377-0257 DOI: http://dx.doi.org/10.1016/0377-0257(96)01439-5.

Sridhar T. e McKinley G.H. Filament-Stretching Rheometry of Complex Fluids [Rivista] // Annual Reviews of Fluid Mechanics. - 2002. - Vol. 38. - p. 375-415.

Starkweather Jr Howard W e Avakian Peter Effect of adsorbed salts on the conductivity of nylon 66 [Rivista] // Macromolecules. - [s.l.] : ACS Publications, 1993. - 23 : Vol. 26. - p. 6217-6219.

Stephens Jean S, Chase D Bruce e Rabolt John F Effect of the electrospinning process on polymer crystallization chain conformation in nylon-6 and nylon-12 [Rivista] // Macromolecules. - [s.l.] : ACS Publications, 2004. - 3 : Vol. 37. - p. 877-881.

Suo Zhigang Evolving small structures [Libro]. - 2004. - Vol. lesson 08.

Valenti B [et al.] Bulk properties of synthetic polymer-inorganic salt systems. Melting behavior of salted poly (caproamide) [Rivista] // The Journal of Physical Chemistry. - [s.l.] : ACS Publications, 1973. - 3 : Vol. 77. - p. 389-395.

Yu Jian H., Fridrikh Sergey V. e Rutledge Gregory C. The role of elasticity in the formation of electrospun fibers [Rivista] // Polymer . - 2006. - 13 : Vol. 47. - p. 4789-4797. - ISSN: 0032-3861 DOI: http://dx.doi.org/10.1016/j.polymer.2006.04.050.

Annex A: CaBER D(t) curves

% FeCl₃

0
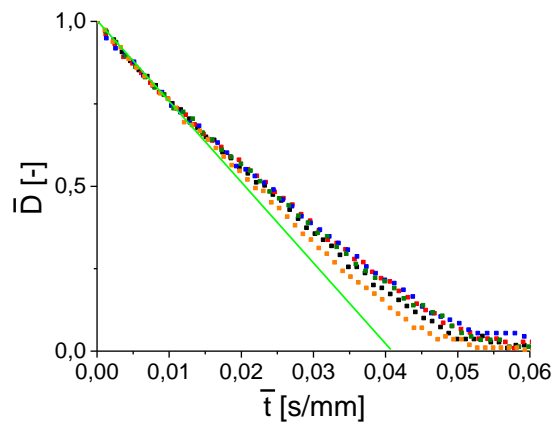
1
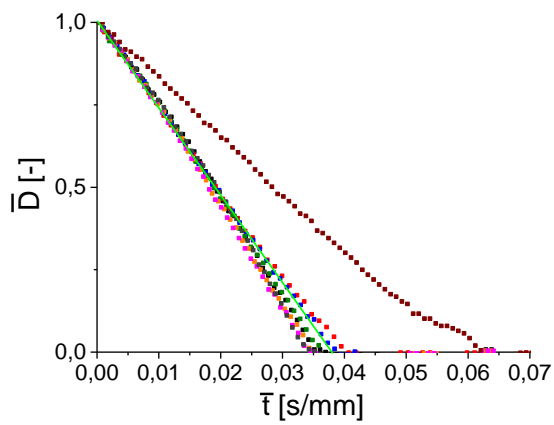
% FeCl₃

1,5

2

2,5

% FeCl₃

3

3,5

4
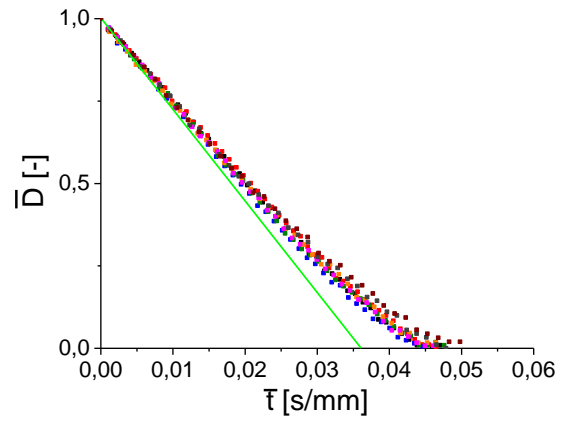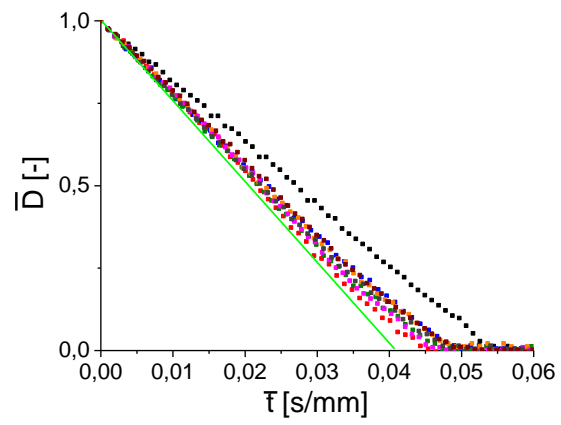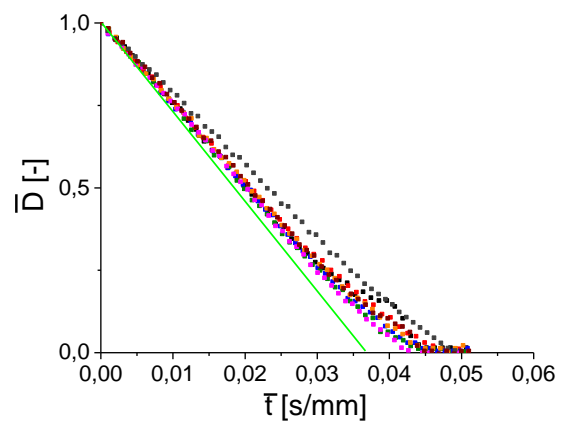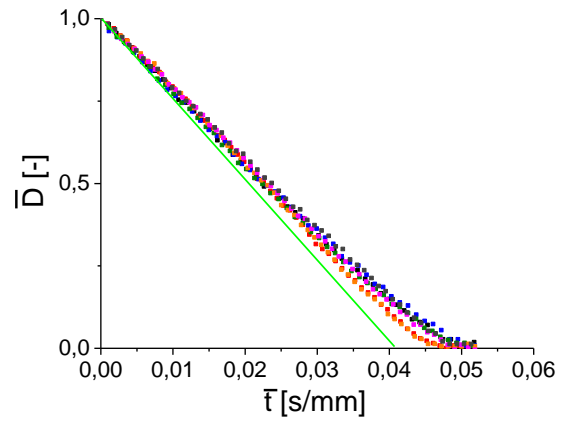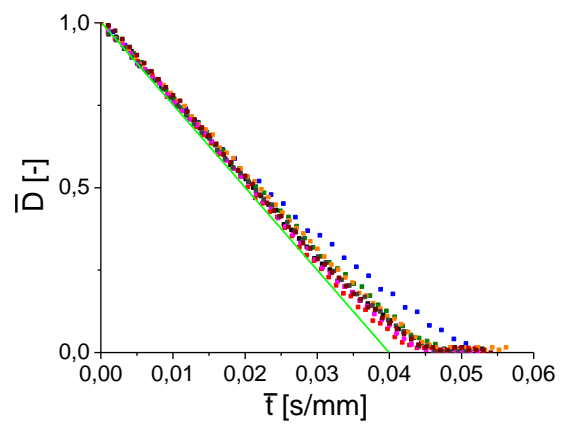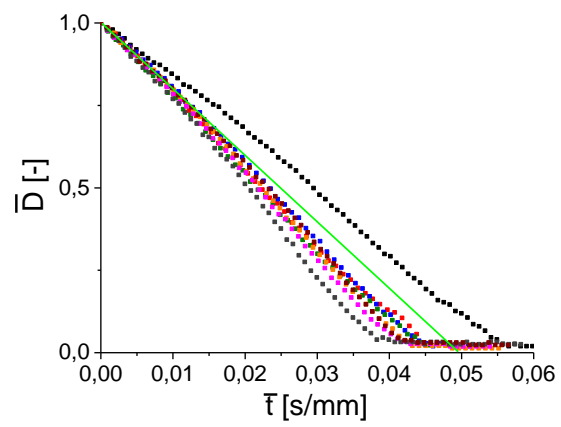
4,5
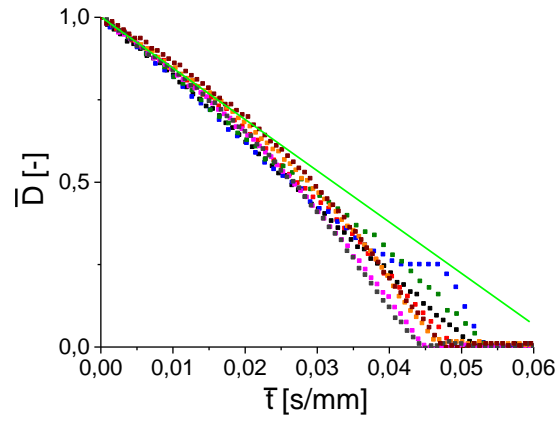
5
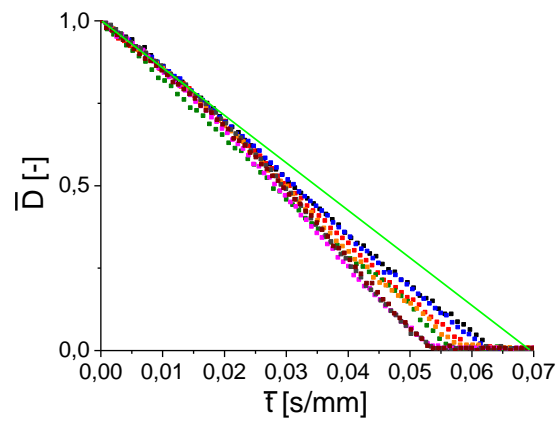
5,5
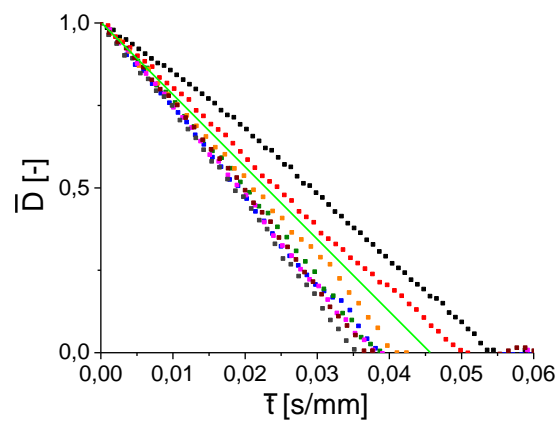
% FeCl₃

5,6
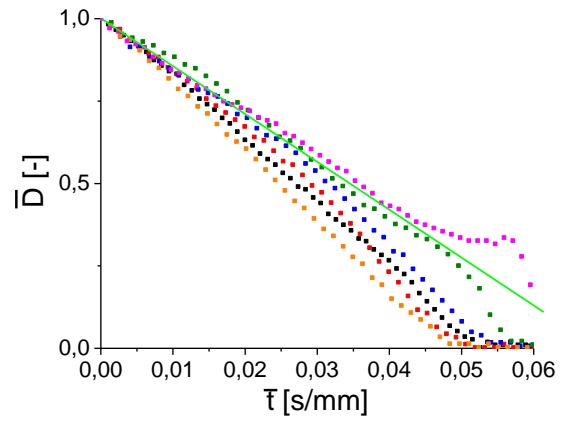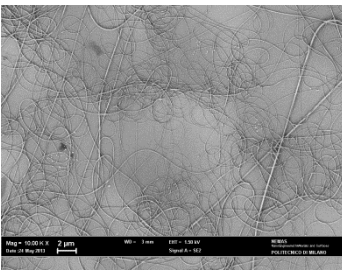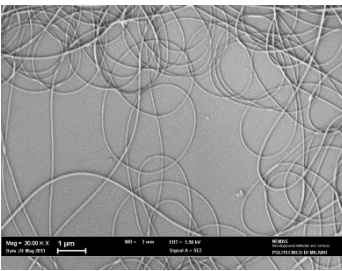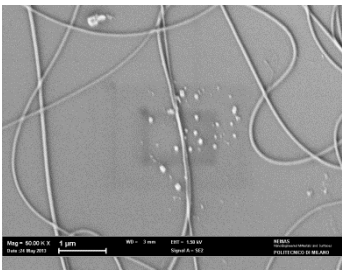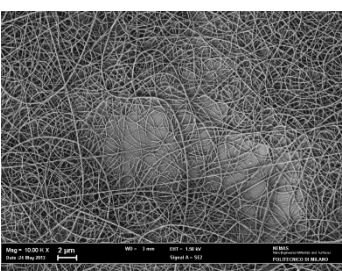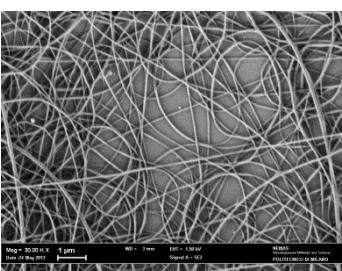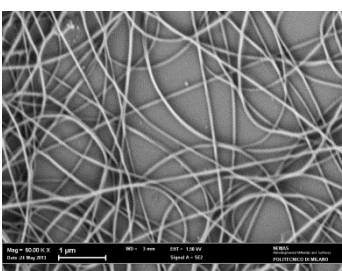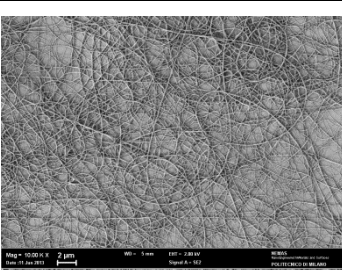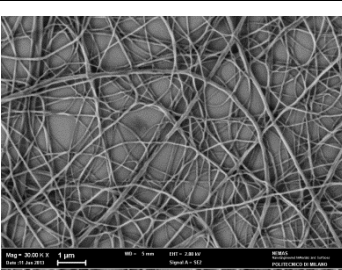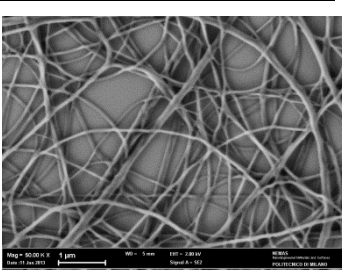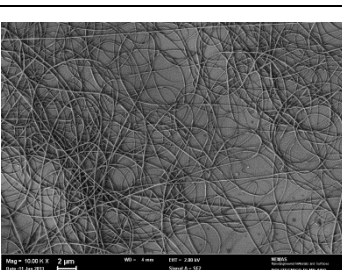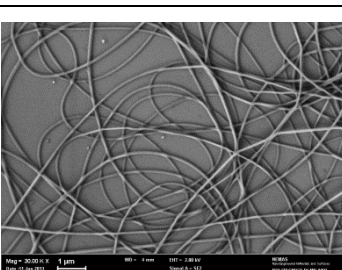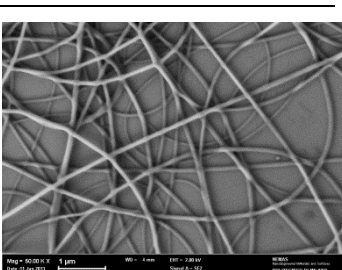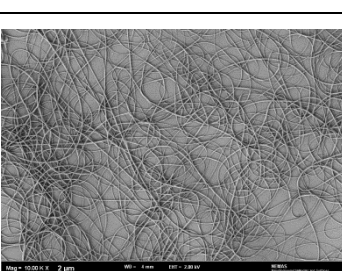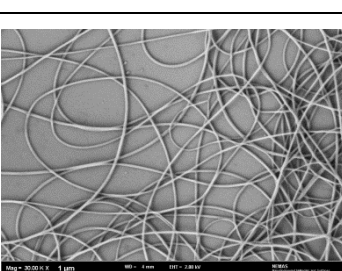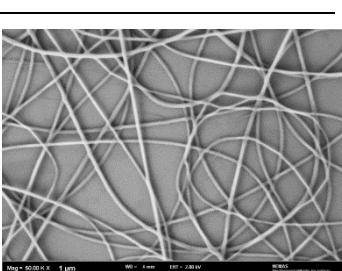
6,5
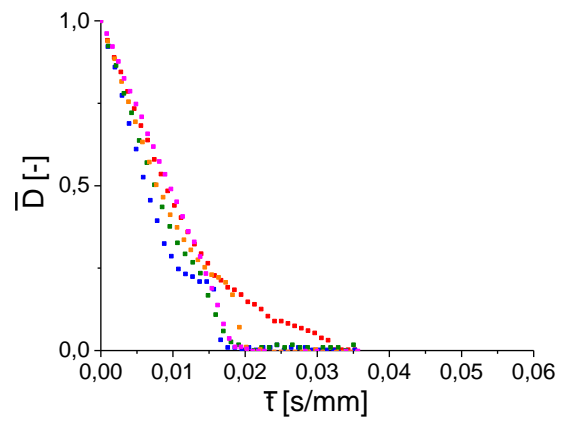
Annex B: SEM images

%FeCl$_3$	5/10 kX	30 kX	50/70/100 kX
0			
1			
1,5			
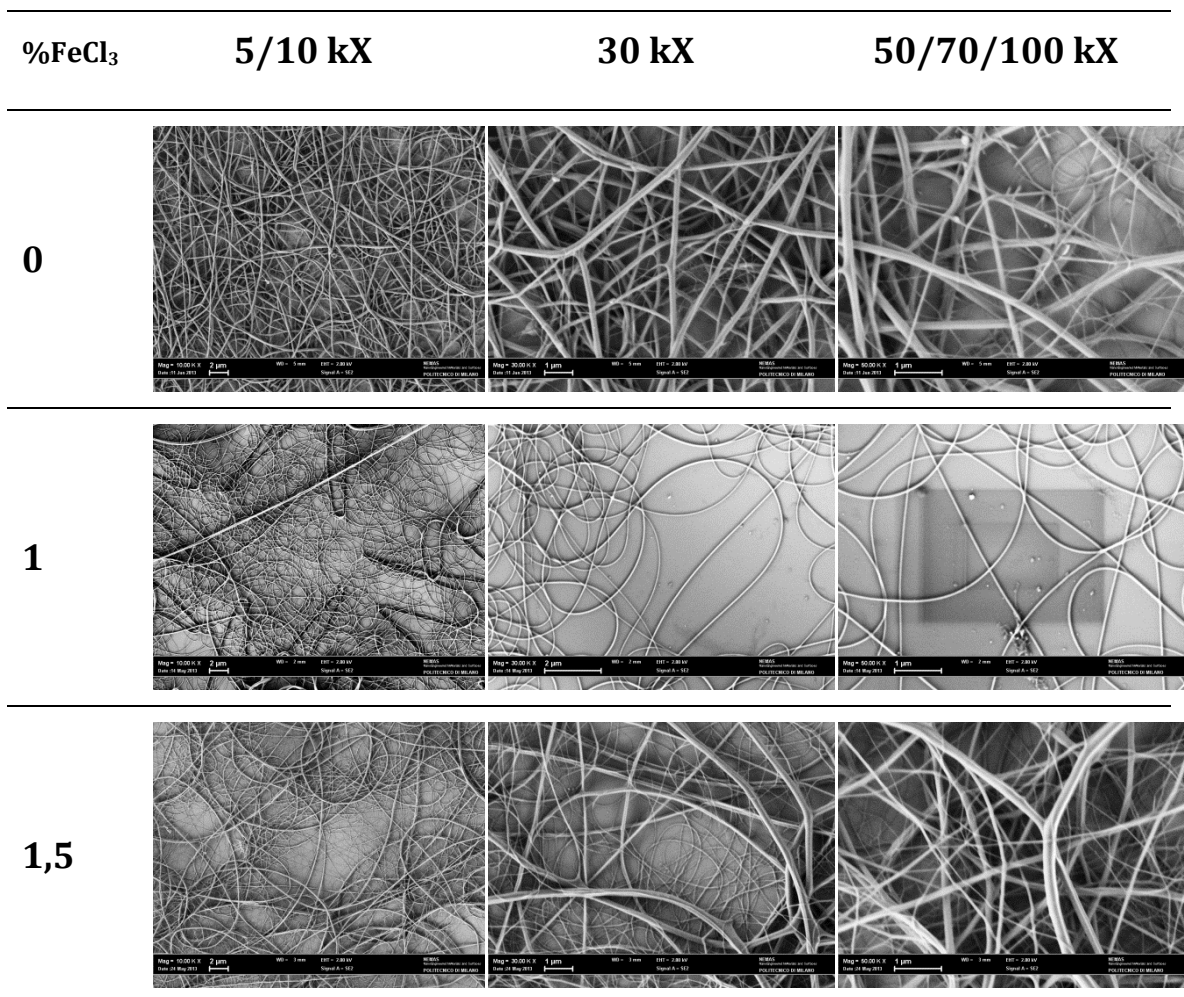
%FeCl₃	5/10 kX	30 kX	50/70/100 kX
2			
2,5			
3			
3,5			
4			

%FeCl₃	5/10 kX	30 kX	50/70/100 kX
4,5			
5			
5,5			
5,6			
6,5			